AD-A124 995 PREDICTION OF NATURAL CONVECTION FLOW PATTERN IN LOW-ASPECT RATIO ENCLOSU..(U) CASE INST OF TECH CLEVELAND OHIO FLUID THERMAL AND AEROSPACE S..

UNCLASSIFIED J LEE ET AL. 26 MAY 82 FTAS/TR-82-158 F/G 12/1 NL

1/2

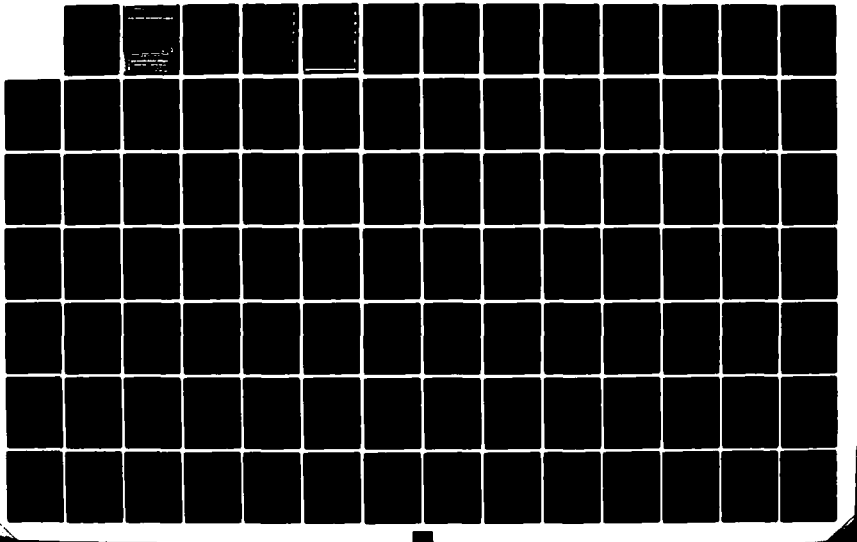

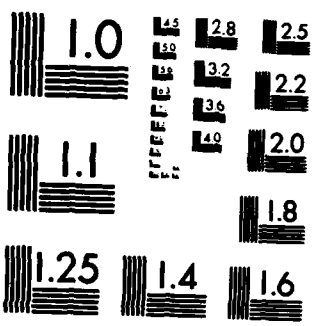

MICROCOPY RESOLUTION TEST CHART
NATIONAL BUREAU OF STANDARDS-1963-A

AD A124955

DTIC

FTAS/TR-82-158

PREDICTION OF NATURAL CONVECTION FLOW PATTERN IN LOW-ASPECT RATIO ENCLOSURES

BY

Jinho Lee and Simon Ostrach

Department of Mechanical and Aerospace Engineering

CASE WESTERN RESERVE UNIVERSITY

Cleveland, Ohio 44106

May 26, 1982

ELECTE
MAR 1 1983
D
A

AIR FORCE OFFICE OF SCIENTIFIC RESEARCH (AFSC)
NOTICE OF TRANSMITTAL TO DTIC
This technical report has been reviewed and is approved for public release IAW AFR 190-12.
Distribution is unlimited.
MATTHEW J. KERPER
Chief, Technical Information Division

SECURITY CLASSIFICATION OF THIS PAGE (When Data Entered)

REPORT DOCUMENTATION PAGE

READ INSTRUCTIONS BEFORE COMPLETING FORM

1. REPORT NUMBER: AFOSR-TR- 83-0031	2. GOVT ACCESSION NO.: AD-A124 993
3. RECIPIENT'S CATALOG NUMBER	
4. TITLE (and Subtitle): PREDICTION OF NATURAL CONVECTION FLOW PATTERN IN LOW-ASPECT RATIO ENCLOSURES	5. TYPE OF REPORT & PERIOD COVERED: INTERIM
	6. PERFORMING ORG. REPORT NUMBER
7. AUTHOR(s): JINHO LEE SIMON OSTRACH	8. CONTRACT OR GRANT NUMBER(s): AFOSR-81-0045
9. PERFORMING ORGANIZATION NAME AND ADDRESS: CASE WESTERN RESERVE UNIVERSITY DEPT OF MECHANICAL & AEROSPACE ENGINEERING CLEVELAND, OH 44106	10. PROGRAM ELEMENT, PROJECT, TASK AREA & WORK UNIT NUMBERS: 61102F 2307/A4
11. CONTROLLING OFFICE NAME AND ADDRESS: AIR FORCE OFFICE OF SCIENTIFIC RESEARCH/NA BOLLING AFB, DC 20332	12. REPORT DATE: May 1982 13. NUMBER OF PAGES: 121
14. MONITORING AGENCY NAME & ADDRESS(if different from Controlling Office)	15. SECURITY CLASS. (of this report): Unclassified 15a. DECLASSIFICATION DOWNGRADING SCHEDULE

16. DISTRIBUTION STATEMENT (of this Report)

Approved for Public Release; Distribution Unlimited.

17. DISTRIBUTION STATEMENT (of the abstract entered in Block 20, if different from Report)

18. SUPPLEMENTARY NOTES

19. KEY WORDS (Continue on reverse side if necessary and identify by block number)

NATURAL CONVECTION
LOW ASPECT RATIO ENCLOSURES
MULTIPLE SCALES TECHNIQUE
PREDICTION OF FLOW PATTERNS

20. ABSTRACT (Continue on reverse side if necessary and identify by block number)

The present work deals with the natural convection of a fluid confined within a low aspect ratio rectangular enclosure with differentially heated end walls. The objective is to predict the core flow pattern a priori once the boundary and geometry conditions are given. Multiple scales technique is employed to obtain a proper mathematical model from which the core flow patterns are analyzed based on various force balances. Global analyses show a number of possible core configurations. Detailed analyses lead to predictions for the occurrence of possible flow subregimes, such as secondary

DD FORM 1 JAN 73 1473 EDITION OF 1 NOV 65 IS OBSOLETE

UNCLASSIFIED
SECURITY CLASSIFICATION OF THIS PAGE (When Data Entered)

cells. Comparison with the existing experimental results shows good agreement.

ABSTRACT

The present work deals with the natural convection of a fluid confined within a low aspect ratio rectangular enclosure with differentially heated end walls. The objective is to predict the core flow pattern a priori once the boundary and geometry conditions are given.

Multiple scales technique is employed to obtain a proper mathematical model from which the core flow patterns are analyzed based on various force balances.

Global analyses show a number of possible core configurations. Detailed analyses lead to predictions for the occurrence of possible flow subregimes, such as secondary cells. Comparison with the existing experimental results shows good agreement.

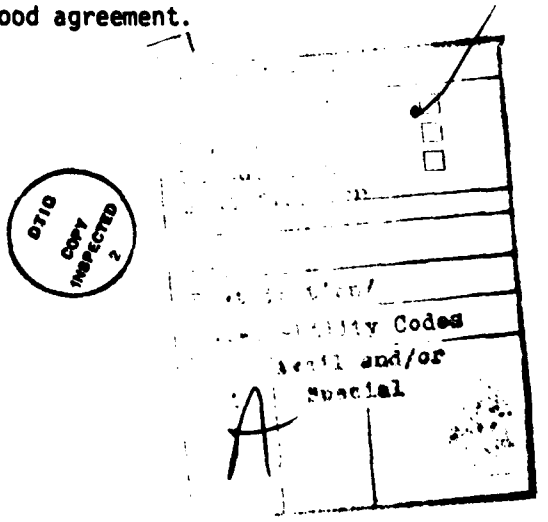

ACKNOWLEDGEMENT

This work was financially supported by the Air Force Office of Scientific Research under Grant No. AFOSR-81-0045.

TABLE OF CONTENTS

LIST OF FIGURES

LIST OF TABLES

LIST OF SYMBOLS

A	Aspect ratio, $\frac{H}{L}$
A_c	Aspect ratio defined as $\frac{h_c}{\ell_c}$
D	Mass diffusivity
g	Acceleration due to gravity
Gr_H	Grashof number based on H, $\frac{\beta g \Delta T H^3}{\nu^2}$
Gr_L	Grashof number based on L, $\frac{\beta g \Delta T L^3}{\nu^2}$
H	Height of the enclosure
h_c	Unspecified vertical length scale for core motion
k	Thermal conductivity
k_i	Constants, i = 1, 2,....
L	Length of the enclosure
ℓ	Unspecified length scale for characteristic vorticity Ξ_R
ℓ_c	Unspecified horizontal length scale for core motion
n	Arbitrary integer approximating the ratio of $\frac{L}{\ell_c}$
Pr	Prandtl number, $\frac{\nu}{\alpha}$
Ra_H	Rayleigh number based on H, $\frac{\beta g \Delta T H^3}{\alpha \nu}$
Ra_L	Rayleigh number based on L, $\frac{\beta g \Delta T L^3}{\alpha \nu}$
S_c	Schmidt number, $\frac{\nu}{D}$
T	Temperature
T_c	Temperature on cooled side wall
T_H	Temperature on heated side wall

ΔT	Imposed temperature difference, $T_H - T_C$
X	Dimensional horizontal coordinate
x	Dimensionless horizontal coordinate
Y	Dimensional vertical coordinate
y	Dimensionless vertical coordinate
$\tilde{y}$	Dimensionless stretched vertical coordinate

GREEK SYMBOLS

α	Thermal diffusivity
β	Coefficient of volumetric thermal expansion
δ_h	Arbitrary horizontal layer in the core
δ_v	Horizontal viscous layer in the core
δ_x	Horizontal characteristic length scale in the end region
δ_y	Horizontal thermal layer in the core
ε_h	Stretching parameter for the vertical coordinate defined in (4.1)
ε_v	Stretching parameter for the vertical coordinate defined in (3.115)
ε_x	Stretching parameter for the horizontal coordinate defined in (2.11)
ε_y	Stretching parameter for the vertical coordinate defined in (3.101)
ζ	Dimensionless horizontal coordinate
η	Dimensionless stretched horizontal coordinate
θ	Dimensionless temperature
ν	Kinematic viscosity

Ξ	Dimensional vorticity
Ξ_R	Characteristic vorticity
ξ	Dimensionless vorticity
Ψ	Dimensional stream function
Ψ_R	Characteristic stream function
$\overline{\Psi}_R$	Modified characteristic stream function
ψ	Dimensionless stream function

SUBSCRIPTS

c	Core or mid-core region
e	End region
i	Inside the horizontal viscous layer
o	Outside the horizontal viscous layer

CHAPTER I

INTRODUCTION

1.1 General Aspects of the Problem

Over the past two decades, convection phenomena induced by body forces have been the object of extensive research efforts. A rather broad classification into two types of problem can be made: The external problem which considers the flow and heat transfer over a body, such as a heated rod or plate, in a fluid at rest and is referred to as free convection. The internal problem which deals with the flow and heat transfer in confined fluids and is referred to as natural convection.

Natural convection in completely confined fluids occurs in many and diverse applications and has, as a result, been receiving more attention recently. The study of natural convection flows that are completely bounded by surfaces leads to a number of difficult problems. Natural convection is extremely sensitive to the configuration and boundary conditions. Theoretical analysis is limited because of the inherent coupling and nonlinearity of the basic equations.

For large Grashof and/or Rayleigh numbers, the flow will obviously be of a boundary layer type. For external problems Prandtl boundary layer theory yields the same simplifications that are helpful in other problems and the region exterior to the boundary layer can be determined once the boundary layer flow is known.

But in a completely enclosed region, the region exterior to the boundary layer will actually be enclosed by the boundary layer and will form what is called the "interior" or the "core region". As the core region is completely surrounded by the boundary layer, the flow in the core is not readily determined from the external boundary conditions but depends on the action of the boundary layer. Hence the boundary layer and core are closely coupled so that it is very difficult to predict the core flow pattern a priori. Since the analytical boundary layer approach does require a priori knowledge of the core configuration at the outset, it is precisely this coupling that constitutes the main source of difficulty in obtaining analytical solutions or even in getting qualitative ideas of the flow patterns to internal problems.

1.2 Review of Existing Work

Since the present work is directed towards those cases in which the fluid is heated-from-side and is mainly concerned with the prediction of flow patterns in the core, existing work will be reviewed in detail from that point of view.

Most of the earlier works were concerned with natural convection in horizontal cylinders and high aspect ratio rectangles. A comprehensive review of earlier existing works has been done by Ostrach [1]. More recent research on natural convection flows in horizontal, vertical and tilted rectangular enclosures was reviewed by Catton [2].

As was pointed out in [1], in the earlier analytical works, e.g., Ostrach [3], Batchelor [4], Weinbaum [5] and Menold and Ostrach [6], except Gill [7] and Hantman [8], the core configuration was, a priori, considered as isothermal and rotating regardless of the thermal boundary conditions. A series of experiments by Ostrach and Pneuli [9], Ostrach and Menold [10], Brooks and Ostrach [11] and Sbazebari and Ostrach [12] showed that the detailed nature of the core flow depends on the thermal boundary conditions. Experiments applicable to the heating-from-side case, e.g., Brooks and Ostrach [11], Sabzebari and Ostrach [12], Martini and Churchill [13], Eckert and Carlson [14], Elder [15], etc. indicated a thermally stratified core with relatively slow flow. With the exception of the work of Poots [16], all the numerical work, e.g, Wilkes and Churchill [17], Elder [18], De Vahl Davis [19], MacGregor and Emery [20], Newell and Schmidt [21], Quon [22], Taylor and Ijan [23], etc. was performed with the experimental work in mind and was in essential agreement with this picture. The failure of the assumption of the isothermal, rotating core for heating-from-side case was brought out especially by the solution of Menold and Ostrach [6]. Although a rotating, isothermal core has not yet been experimentally observed for heating-from-side case, the possibility of its occurring and other patterns too may not be dismissed.

In contrast with the considerable work done on natural convection in horizontal circular cylinders and high aspect ratio

rectangles, it is rather surprising that relatively little work has been done on natural convection in enclosures with low aspect ratio even though this problem has many engineering applications.

Boyack and Kearney [24] first obtained numerical results for a low aspect ratio rectangle and emphasized the need to study natural convection processes for application to auxiliary cooling equipment of high temperature gas cooled reactors and solar collectors.

Solan and Ostrach [25] discussed the need for understanding such phenomena in order to improve the growth of crystals by closed-tube vapor deposition.

In 1973, Klosse and Ullersma [26] considered a gas in a two-dimensional low aspect ratio rectangular enclosure using fully-developed flow as the base and, as essentially assumed, an S-shaped velocity profile was found in the central region of the enclosure with vertical flows in the end regions.

Later, Cormack, Leal, Imberger and Seinfeld [27] ∿[29] studied buoyancy driven convection in shallow lakes as a shallow cavity problem analytically, numerically and experimentally, respectively.

In the analytical work of Cormack et. al. [27], they investigated the problem when the aspect ratio, A, goes to very small value with arbitrary but fixed Grashof number, Gr_H, by the matched asymptotic expansion method. Their results show that when $A \to 0$, the flow consists of two distinct regimes, a parallel flow in the core region and a second, non-parallel flow near the end of the

cavity. They also show that the primary driving force for the motion is the horizontal temperature gradient in the core and the temperature distribution to the first order in the aspect ratio, A, in the cavity is strictly linear in the horizontal direction. Thus the dominant mode of heat transfer is pure conduction. However, they could not indicate explicitly the upper limit of Gr_H within which their solution is valid. They just gave an approximate criterion by requiring only that the second term in the expansion for K_1, the single parameter of the parallel flow solution, be small relative to the first, i.e., $Gr_H^2 Pr^2 A^3 \lesssim 10^5$. A comparison of numerical solutions of Cormack, Leal and Seinfeld [28] with the asymptotic theory shows excellent agreement among the analytical and numerical solutions proved that $A \lesssim 0.1$ and $Gr_H^2 Pr^2 A^3 \lesssim 10^5$. In addition, the numerical solutions also demonstrate the transition from the parallel flow regime to the boundary layer limit; for A fixed, $Gr_H \to \infty$. In Imberger's experiment [29], most of the flow features mentioned in numerical work were also qualitatively present in the experimental flows. But when $Gr_H^2 Pr^2 A^3$ becomes nearly 10^{11}, the mid-depth becomes an isotherm and there is a slow central circulation throughout the whole cavity, which is absent in the much larger aspect ratios. Therefore it was pointed out in [29] that it was uncertain whether the limit $Ra_H \to \infty$ is different for A small and A large. In this respect, it was also pointed out that the theory developed in [27] for small values of $Ra_H^2 A^3$ is inappropriate in the sense that it predicts parallel flow in the core

region for all values of the Rayleigh number.

Bejan and Tien [30] considered the case of small, fixed A with Ra_H variable. They developed three characteristic flow regimes with respect to the value of Ra_H and derived a set of analytical results for the Nusselt number corresponding to each flow regime. They assumed the existence of parallel flows in the core in all three regimes, but this is not true under certain conditions. In the experiments of Ostrach et. al. [31], Al-Homoud [32], and Kamotani et. al. [33], many different core configurations were observed. Therefore their predictions are of limited and undefined validity.

In the experiment of Ostrach et. al. [31], it is indicated that for the range of aspect ratios and Grashof and Prandtl numbers covered, i.e., $0.05 \lesssim A \lesssim 0.5$., $27.7 \lesssim Gr_H \lesssim 10^6$ and $0.72 \lesssim Pr \lesssim 1.38 \times 10^3$, the flow pattern is predominantly unicellular and parallel for the aspect ratios of 0.1 and smaller. Secondary cells are observed near the enclosure ends when the aspect ratio is 0.2 and $(Gr_H PrA)^2$ is of the order of 10^{13} for Prandtl numbers of the order of 10^3, where the horizontal boundaries are semi-conducting.

In Al-Homoud's experiment [32] with water, it is shown that in the range of $2 \times 10^8 < Ra_H < 2 \times 10^9$ and A = 0.0625, the core flow structure is non-parallel and is dominated by horizontal intrusions flowing along each of the two insulated horizontal walls of the enclosure and the fluid embraced by the two horizontal jets is practically stagnant and thermally stratified.

Sernas and Lee [34, 35] investigated the heat transfer in a rectangular air enclosure both interferometrically and numerically. In [34], they investigated interferometrically air in enclosures for the range $0.1 \lesssim A \lesssim 1.0$ and $2.64 \times 10^6 \lesssim Gr_L \lesssim 5.45 \times 10^6$. Their enclosures were composed of two types of horizontal boundaries. One type was made for isothermal horizontal boundary conditions and the other type for adiabatic horizontal boundary conditions. Heat transfer characteristics and flow patterns within these two types of enclosures were found to be significantly different for the experimental range covered. In [35], they investigated the problem numerically for air with $0.1 \lesssim A \lesssim 1.0$ and $10^6 \lesssim Gr_L \lesssim 3 \times 10^7$. When A = 0.1, the isotherms and streamlines in the isothermal enclosure become very much different from those in the adiabatic enclosure in contrast with the case of A = 1.0 and 0.4 in which the patterns were very similar to each other. When A = 0.1, the flow pattern in the core region is nearly parallel in the adiabatic enclosure while in the isothermal enclosure, there is almost no fluid motion in the core except near the end region.

Tseng [36] presented some numerical results for slightly low aspect ratio rectangles in his work on tilted rectangular enclosures with adiabatic, isothermal and perfectly conductive connecting walls at $10^4 \lesssim Ra_L \lesssim 9 \times 10^7$, $0.1 \lesssim Pr \lesssim 100$ and $-90° \lesssim \phi \lesssim 80°$, For $Ra_L = 10^6$, A = 0.5 and $\phi = 0°$, no appreciable distinctions are observed in the isotherms and streamline distributions among those three kinds of connecting walls.

Patterson and Imberger [37] recently considered the problem of transient natural convection in a cavity of $A \lesssim 1$. Scale analysis is used to show that a number of initial flow types are possible, collapsing ultimately into two basic types of steady flow, conduction dominant flow and convective flow, determined by the relative value of the non-dimensional parameters describing the flow. A number of numerical solutions which encompass both flow types are obtained, and their relationship to the scale analysis is discussed.

More recently Kamotani et. al. [33] give a comprehensive picture of natural convection heat transfer in low aspect ratio enclosures by systematically varying the parameters Ra_H, A and Pr. Among the experimental results, secondary cells are present in the end region for A = 0.2, $Ra_H = 4.8 \times 10^4$ and Pr = 965 and are shown to influence the Nusselt number noticeably. In such a case, the core flow pattern was not parallel.

Most recently, Simpkins and Dudderar [38] experimentally studied convection in rectangular cavity for a variety of Rayleigh numbers and aspect ratios for fluids with Prandtl number $Pr \gtrsim 10$. For small aspect ratios, e.g., for A = 0.25, secondary rolls are present and remain near the outer edge of the vertical boundary layers and the motion between them becomes disordered. There is no evidence of more than two secondary rolls appearing in the cavity. The critical Rayleigh number for secondary rolls is given by

$$(Ra_H)_c A^{3/4} \sim 6.4 \times 10^5 \pm 10\ \% \qquad (1.1)$$

Their observations also suggest that the horizontal boundary layers have a significant effect on the core flow field.

Shiralkar and Tien [39] investigated numerically heat transfer by natural convection in a horizontal cavity for low aspect ratios. Numerical results have been obtained for Pr = 1.0, $0.025 \leq A \leq 1.0$ and $Ra_H \leq 6 \times 10^6$ and for A = 0.1, $0.01 \leq Pr \leq 100$ and $Ra_H \leq 10^6$. For high and moderate Pr, the structure of flow in the core reveals essentially parallel streamlines. Nusselt number shows good agreement with the prediction of Bejan and Tien [30] at high and low Ra_H. In the intermediate range, the agreement is poor. The numerical results also indicate that for low Pr, even at A = 0.1, at $Ra_H = 10^6$, the core flow is not fully developed; on the contrary, the core contains developing velocity boundary layers along the horizontal walls.

In addition, Jhaveri and Rosenberger [40] also studied numerically thermal convection in a vapor transport process across a horizontal rectangular enclosure for A = 0.1, Sc = 0.5, Pr = 0.7 a d $Gr_H \leq 3.3 \times 10^4$, which was earlier considered rather simply by Klosse and Ullersma [26]. Many of the simplifying assumptions made in [26] were not used in [40]. The problem of interest in [40] includes the effect of mass flux as well as heat flux and it is assumed that buoyancy is due primarily to temperature differences. However, the boundary conditions differ from the pure natural convection flows because of the concentration difference. In that, the horizontal mass average velocity at the interfaces is

specified in terms of mass flux through Fick's law. The flow profiles determined in this way indicate the onset of a recirculation cell at each interface for $Gr_H = 3.3 \times 10^4$. It should be noted that the cell is due to the coupling of mass flux at the interfaces with the transport equations, otherwise the modeled systems just reduce to the pure natural convection problem.

1.3 Motivation of the Present Work

As is pointed out in [1], in the confined natural convection problems in horizontal cylinders and high aspect ratio rectangles, two core configurations are mathematically possible, viz., rotating and isothermal or stagnant and stratified. Analytical and numerical solutions first indicated the former and it was only after experiments indicated that the latter always occurred that such results were obtained theoretically. Similarly, in the low aspect ratio rectangular enclosures, it was shown experimentally that the flow structure in the core is not always parallel. Under certain conditions, there appeared other types of core configurations such as secondary cells or stagnation flows in the core. Such ambiguities concerning the nature of the flows are inherent in all internal convection problems as has been shown above and there does not, as yet, exist any way of predicting with confidence, a priori, what the core flow pattern will be.

The primary motivation of the present work is to develop some means to predict the core flow patterns in low aspect ratio

rectangular enclosures.

1.4 Method of Approach

In a low aspect ratio rectangular enclosure, the flow region can essentially be divided into two regions. One, the region near end walls which we will call herein "end region" and the other, "core region", the region outside the end region with horizontal boundaries.

In order to be able to predict the core flow pattern, and thus, the whole flow pattern correctly, one has to be clear on what physical mechanisms govern the core flow. To do this, one has to develop a mathematical model which properly represents the physics of the core flow.

Since the flow characteristics may be different and coupled in each flow region, it is not possible to consider all the important physical mechanisms in the enclosure by the governing equations based on either one region. In addition, the equations that describe the phenomena of interest herein are non-linear and bidirectionally coupled. Any simplifications must, therefore, be carefully made. In order to ensure that an assumption made in one equation is consistently transmitted to the other equations, a somewhat formal procedure is employed herein based on the method of multiple scales. Multiple scales are introduced to give mathematical degrees of freedom which enable physical statements to be properly made on the important physical mechanisms in the enclosure.

Analytically the method of multiple scales can be used to obtain single uniformly valid expansions, in contrast with the method of matched asymptotic expansions which yields two expansions that must be matched [Nayfeh (41)].

Based on the scaling analysis which gives degrees of freedom, proper force balances in the basic dimensionless equations can be made and the order of magnitude of each physical terms can be estimated with the relevant dimensionless parameter as its coefficient. Then, by considering the derivatives with respect to core flow region, the equations which will describe the core flow characteristics can be extracted from the basic dimensionless equations. The core flow patterns are first studied in a global sense under the implicit assumption that there exist no flow subregimes, such as secondary cells. On that basis, the geometric length scales are the proper ones for the core flow structure. With the use of the results of the global considerations, detailed analysis is made to determine the possibility of flow subregimes. In the detailed analysis, arbitrary length scales replace the geometric length scales in the dimensionless equations.

In an attempt to predict the core flow patterns in the detailed analysis, no criteria could be found for the presence of closed streamlines in the core which would yield the necessary and sufficient conditions for the occurrence of secondary cells. Instead, the occurrence of flow subregimes is considered to be possible herein when the arbitrary horizontal length scale, ℓ_c, is less than

the geometric length scale, L, i.e., $\frac{\ell_c}{L} < 1$. This statement may not be the sufficient condition, but, at least it can be considered to be a necessary condition for the occurrence of flow subregimes. The results obtained on this premise are compared with existing experimental data.

CHAPTER II

MATHEMATICAL FORMULATION OF THE PROBLEM

The problem to be studied herein is the convective motion of a fluid driven by the imposed temperature difference between the end walls within a two-dimensional rectangular enclosure of length L and height H. The schematic diagram of the system is shown in Fig. 1.

The flow field will be considered to be steady, two-dimensional, laminar and quasi-incompressible. By quasi-incompressibility it is meant that the variations in density due to temperature differences are neglected except where they modify the body force terms in the momentum equations. This is generally referred to as Boussinesq approximation and has been discussed in a formal way by Ostrach [42].

2.1 Normalization of the Basic Equations

The basic equations of vorticity and energy transport for two-dimensional flow can be written as

$$\frac{\partial(\Xi, \Psi)}{\partial(X, Y)} = \beta g \frac{\partial T}{\partial X} + \nu \left(\frac{\partial^2 \Xi}{\partial X^2} + \frac{\partial^2 \Xi}{\partial Y^2} \right) \tag{2.1}$$

$$\Xi = - \left(\frac{\partial^2 \Psi}{\partial X^2} + \frac{\partial^2 \Psi}{\partial Y^2} \right) \tag{2.2}$$

$$\frac{\partial(T, \Psi)}{\partial(X, Y)} = \alpha \left(\frac{\partial^2 T}{\partial X^2} + \frac{\partial^2 T}{\partial Y^2} \right) \tag{2.3}$$

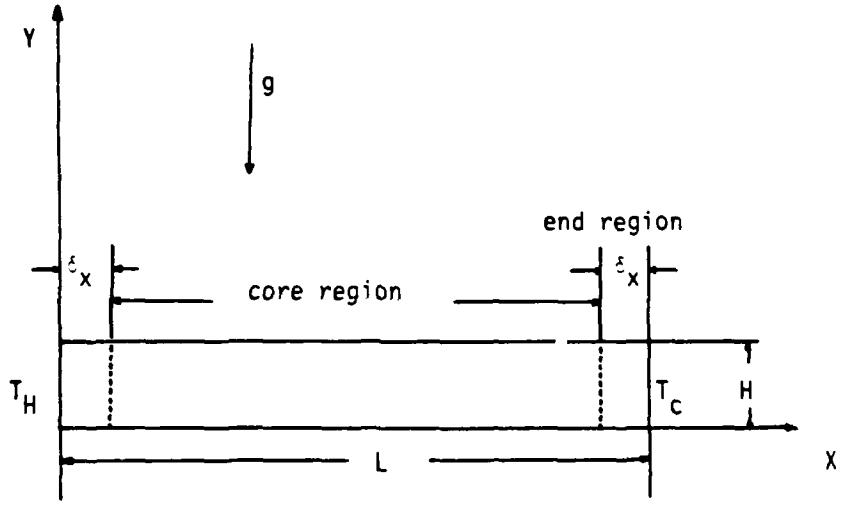

Figure 1. Schematic Diagram of the System

where Ξ denotes vorticity, Ψ the stream function and T temperature. Also g is the acceleration due to gravity and ν, β and α, the kinematic viscosity, coefficient of thermal expansion and thermal diffusivity.

The viscous dissipation was neglected in the energy equation (2.3) due mainly to the very low velocities present in natural convection flows of the type considered herein. The variations of the dynamic viscosity ν and thermal conductivity k were also neglected as a result of the quasi-incompressiblity of the fluid.

The corresponding boundary conditions are

$$\Psi = \frac{\partial \Psi}{\partial X} = 0 , \quad T = T_H, T_c \qquad \text{at } X = 0, L \tag{2.4a}$$

$$\Psi = \frac{\partial \Psi}{\partial Y} = 0 , \quad \frac{\partial T}{\partial Y} = 0 \qquad \text{at } Y = 0, H \tag{2.4b}$$

The basic equations (2.1) to (2.3) are made dimensionless by the following definitions.

$$x = \frac{X}{L} , \quad y = \frac{Y}{H} , \quad \psi = \frac{\Psi}{\Psi_R}$$
$$\xi = \frac{\Xi}{\Xi_R} = \frac{\Xi}{\Psi_R/\ell^2} , \quad \theta = \frac{T-T_c}{T_H-T_c} \tag{2.5}$$

In (2.5), the characteristic stream function Ψ_R is to be specified later in the analysis in accordance with the physics of the problem. The characteristic vorticity Ξ_R is represented as Ψ_R/ℓ^2, where ℓ is a length scale that will also be specified in the course of analysis. The purpose of introducing the unspecified length scale ℓ

(instead of using the specific geometric length scale) is to normalize the vorticity properly according to the physical situation of the system.

Substitution of the definitions (2.5) into eqs. (2.1) ∿ (2.3) yields

$$\frac{\partial(\xi,\psi)}{\partial(x,y)} = \frac{\beta g \Delta T H \ell^2}{\nu_R^2}\frac{\partial\theta}{\partial x} + \frac{\nu L}{\nu_R H}\left(A^2\frac{\partial^2\xi}{\partial x^2} + \frac{\partial^2\xi}{\partial y^2}\right) \tag{2.6}$$

$$\xi = -\frac{\ell^2}{H^2}\left(A^2\frac{\partial^2\psi}{\partial x^2} + \frac{\partial^2\psi}{\partial y^2}\right) \tag{2.7}$$

$$\frac{\partial(\theta,\psi)}{\partial(x,y)} = \frac{\alpha L}{\nu_R H}\left(A^2\frac{\partial^2\theta}{\partial x^2} + \frac{\partial^2\theta}{\partial y^2}\right) \tag{2.8}$$

where $\Delta T = T_H - T_C$ and A represents the aspect ratio, $\frac{H}{L}$.
The corresponding boundary conditions (2.4) become

$$\psi = \frac{\partial\psi}{\partial x} = 0, \quad \theta = 1, 0 \qquad \text{at } x = 0, 1 \tag{2.9a}$$

$$\psi = \frac{\partial\psi}{\partial y} = 0, \quad \frac{\partial\theta}{\partial y} = 0 \qquad \text{at } y = 0, 1 \tag{2.9b}$$

One property to be pointed out herein is that for adiabatic (or insulated) horizontal boundaries, the equations and boundary conditions have a symmetry property involving reflections about x = 1/2, y = 1/2 of the cavity. This was termed the centro-symmetry property of the equations and boundary conditions by Gill [7], and can be represented as

$$\psi(x,y) = \psi(1-x, 1-y) \tag{2.10a}$$

$$\theta(x,y) = 1 - \theta(1-x, 1-y) \tag{2.10b}$$

2.2 Working Form of the Equations

In the dimensionless equations (2.6) ∿ (2.8), when $A^2 << 1$, the x-direction diffusion terms can be neglected compared to the y-direction diffusion terms. Since the x-direction diffusion terms are the highest order x-derivatives, if they are neglected, the end wall boundary conditions can not be satisfied. Therefore, the equations without the horizontal diffusion terms in Eqs. (2.6) ∿ (2.8) are only valid away from the ends, i.e., in the core. On the other hand, the equations which represent the flow characteristics in the end region could be obtained by properly stretching the x-coordinate in the Eqs. (2.6) ∿(2.8).

In order to obtain insights into the nature of flow characteristics, the unspecified characteristic quantities such as Ψ_R and ℓ in the Eqs. (2.6) ∿ (2.8) first should be determined to see what the relevant dimensionless parameters are. These quantities may, in principle, be determined by considering the flow mechanisms in either region. However, as the two regions are closely coupled and this coupling affects much of the flow structure, it is necessary

that in determining the characteristic quantities, both flow regions and their coupling be considered in some way. Otherwise, some important physical mechanisms may be overlooked by neglecting the coupling effects on the flow characteristics. A mathematically formal procedure is, therefore, employed based on the method of multiple scales through which both the end and core flow regions together with the interacting region are explicitly identified in the basic dimensionless equations.

Here the physical domain of interest is confined and finite and the singular behaviour of the dimensionless equations are expected near the end walls. Thus the multiple scales are introduced in the following way.

$$\zeta = x \quad , \quad \eta = \frac{x}{\varepsilon_x} \tag{2.11}$$

and the derivatives are

$$\frac{\partial}{\partial x} = \frac{1}{\varepsilon_x}\frac{\partial}{\partial \eta} + \frac{\partial}{\partial \zeta} \tag{2.12}$$

$$\frac{\partial^2}{\partial x^2} = \frac{1}{\varepsilon_x^2}\frac{\partial^2}{\partial \eta^2} + \frac{2}{\varepsilon_x}\frac{\partial^2}{\partial \eta \partial \zeta} + \frac{\partial^2}{\partial \zeta^2}$$

where the derivatives with respect to ζ and η represent the core and end region characteristics respectively and ε_x is the small, stretching parameter.

Introducing the derivatives of multiple scales (2.12) into the dimensionless equations (2.6) $\sim$ (2.8), we then obtain

$$\frac{1}{\varepsilon_x}\frac{\partial(\zeta,\psi)}{\partial(\eta,y)} + \frac{\partial(\zeta,\psi)}{\partial(x,y)} = \frac{\beta g \Delta T \ell^2 H}{\nu_R^2}\left(\frac{1}{\varepsilon_x}\frac{\partial\theta}{\partial\eta} + \frac{\partial\theta}{\partial x}\right)$$

$$+ \frac{\nu L}{\nu_R H}\left(\frac{A^2}{\varepsilon_x^2}\frac{\partial^2\zeta}{\partial\eta^2} + 2\frac{A^2}{\varepsilon_x}\frac{\partial^2\zeta}{\partial\eta\partial x} + A^2\frac{\partial^2\zeta}{\partial x^2} + \frac{\partial^2\zeta}{\partial y^2}\right) \tag{2.13}$$

$$\zeta = -\frac{\ell^2}{H^2}\left(\frac{A^2}{\varepsilon_x^2}\frac{\partial^2\psi}{\partial\eta^2} + 2\frac{A^2}{\varepsilon_x}\frac{\partial^2\psi}{\partial\eta\partial x} + A^2\frac{\partial^2\psi}{\partial x^2} + \frac{\partial^2\psi}{\partial y^2}\right) \tag{2.14}$$

$$\frac{1}{\varepsilon_x}\frac{\partial(\theta,\psi)}{\partial(\eta,y)} + \frac{\partial(\theta,\psi)}{\partial(x,y)} = \frac{\alpha L}{\nu_R H}\left(\frac{A^2}{\varepsilon_x^2}\frac{\partial^2\theta}{\partial\eta^2} + 2\frac{A^2}{\varepsilon_x}\frac{\partial^2\theta}{\partial\eta\partial x} + A^2\frac{\partial^2\theta}{\partial x^2} + \frac{\partial^2\theta}{\partial y^2}\right) \tag{2.15}$$

Those are the working form of the basic dimensionless equations.

In the above equations, it is possible that the extent of the end region may be different for the temperature and vorticity distributions. This introduces some ambiguity in ε_x used in the coordinate stretching. It thus should be kept in mind that η is not a normalized variable that always yields the proper normalization of each term in the end region and must, therefore, be carefully treated. Some modification will be made if necessary for the proper normalization in accordance with the physical situation concerned therein.

In the following analysis, the dimensionless groups are first to be determined according to three different cases of force balances in Eqs. (2.13) $\sim$ (2.15). Then the core flow characteristics are going to be studied from a global view by first noting the character of the dimensionless groups, then observing their effects on the equations as they are allowed to take on limiting values.

Finally, the core flow pattern will be examined in detail with the information obtained from the global analysis.

CHAPTER III

GLOBAL VIEW OF THE FLOW CHARACTERISTICS

CASE I: Balance Between Buoyancy and Viscous Forces in the Core

For a given fluid and geometry, when there exist no distinct thermal layers at the end walls within which most of the temperature change occurs, the imposed temperature gradient will be felt across the entire configuration. Since the driving force of the fluid motion concerned herein is the buoyancy force induced only by the temperature gradient, in this situation for low aspect ratio enclosures, i.e., for $A^2 << 1$, the driving force will be the buoyancy force in the core. We therefore study this situation first considering the balance between buoyancy and viscous forces in the core. The explicit conditions for each situation concerned herein will be delineated in the course of analysis.

3.1.1 Basic Equations

From Eq. (2.13), the balance between buoyancy and viscous force in the core can be represented as

$$\frac{\beta g \Delta T \ell^2 H}{\psi_R^2} \sim \frac{\nu L}{\psi_R H} \tag{3.1}$$

Considering that the buoyancy force in the core drives the core flow and that there is not supposed to exist any particular region in the core within which the viscous forces are so concen-

centrated as to balance the core flow, it is appropriate to represent the characteristic vorticity Ξ_R , by specifying the characteristic length ℓ as H, as

$$\ell \sim H \tag{3.2a}$$

and

$$\Xi_R \sim \frac{\Psi_R}{H^2} \tag{3.2b}$$

From (3.1) and (3.2), we obtain

$$\bar{\Psi}_R \sim \frac{\beta g \Delta T H^4}{\nu L} \tag{3.3}$$

One more balance is required here to determine the stretching parameter, ϵ_x, from which the end region flow equations and its characteristic length can be determined. However, at this moment, that is not clear before we know the physics of the core flow properly. Thus this will be considered later after studying the core flow characteristics.

Substituting (3.3) into Eqs. (2.13) ∿ (2.15) and considering the terms with ζ and y derivatives, the equations which will describe the core flow characteristics can be written as

$$Gr_H A^2 \frac{\partial(\Xi,\Psi)}{\partial(\zeta,y)} = \frac{\partial\theta}{\partial\zeta} + A^2\frac{\partial^2\Xi}{\partial\zeta^2} + \frac{\partial^2\Xi}{\partial y^2} \tag{3.4}$$

$$\Xi = -\left(A^2\frac{\partial^2\Psi}{\partial\zeta^2} + \frac{\partial^2\Psi}{\partial y^2}\right) \tag{3.5}$$

$$Pr\,Gr_H A^2 \frac{\partial(\theta,\Psi)}{\partial(\zeta,y)} = A^2\frac{\partial^2\theta}{\partial\zeta^2} + \frac{\partial^2\theta}{\partial y^2} \tag{3.6}$$

For the situation described above, it is now evident that our analysis is valid under the condition $Gr_H A^2 \lesssim 1$. Beyond this condition, i.e., for $Gr_H A^2 >> 1$, inertia becomes dominant in the core, and thus, different scalings are required based on different force balances for the analysis of those situations.

Based on the dimensionless parameters of Eqs. (3.4) ~ (3.6), we are going to study the core flow characteristics. After that, some consideration will be given on the end region based on the core configurations.

3.1.2 Core Flow Characteristics

[1] $Gr_H A^2 << 1$, $A^2 << 1$

Under this condition, the core flow equations (3.4) ~ (3.6) reduce to

$$0 = \frac{\partial \theta}{\partial \zeta} + \frac{\partial^2 \xi}{\partial y^2} \tag{3.7}$$

$$\xi = -\frac{\partial^2 \psi}{\partial y^2} \tag{3.8}$$

$$Pr\,Gr_H A^2 \frac{\partial(\theta, \psi)}{\partial(\zeta, y)} = \frac{\partial^2 \theta}{\partial y^2} \tag{3.9}$$

Because Pr appears as a parameter in Eq. (3.9), its effect must be analyzed. We thus examine the flow characteristics according to Pr.

(i) $\underline{Pr \lesssim 1 \rightarrow Ra_H A^2 << 1}$

When $Pr \lesssim 1$ such that $Ra_H A^2 << 1$, from Eq. (3.9)

$$0 = \frac{\partial^2 \theta}{\partial y^2} \tag{3.10}$$

Considering the adiabatic horizontal boundary conditions (2.9b)

$$\theta = \theta(\zeta) \tag{3.11}$$

Since the buoyancy term in the core, $\frac{\partial \theta}{\partial \zeta}$, in Eq. (3.7) depends on the variation of ζ, its dependence on ζ should be known to obtain the core streamline profiles. From (3.11), considering that the heat flow is one-dimensional in a purely conductive regime, i.e., one-dimensional conduction heat transfer, θ should be linear with respect to ζ as

$$\theta = K_1 \zeta + K_2 \tag{3.12}$$

where k_1 and k_2 are arbitrary constants.

From Eqs. (3.7), (3.8) and (3.12), we then have

$$\frac{d\theta}{d\zeta} = \frac{\partial^4 \psi}{\partial y^4} = K_1 \tag{3.13}$$

Considering the boundary conditions (2.9b), from (3.13) ψ can

be represented

$$\psi = \frac{K_1}{24} y^2 (y-1)^2 \tag{3.14}$$

From (3.12) and (3.14), it is seen that the temperature gradient in the core which provides the driving force for the core flow is linear and the corresponding core flow pattern is parallel.

(ii) $\underline{Pr >> 1 \rightarrow Ra_H A^2 \sim 1}$

When Pr is large such that $Ra_H A^2 \sim 1$, Eq. (3.9) reduces to

$$\frac{\partial(\theta,\psi)}{\partial(\xi,y)} = \frac{\partial^2\theta}{\partial y^2} \tag{3.15}$$

Since the flow characteristics from Eq. (3.15) are not readily perceivable, we try to get information from an integral form of Eq. (3.15) with the boundary conditions at the horizontal boundaries.

If we rewrite Eq. (3.15)

$$\frac{\partial}{\partial\xi}\left(\theta\frac{\partial\psi}{\partial y}\right) + \frac{\partial}{\partial y}\left(-\theta\frac{\partial\psi}{\partial\xi} - \frac{\partial\theta}{\partial y}\right) = 0 \tag{3.16}$$

Integration of Eq. (3.16) with respect to y from y = 0 to 1 yields

$$\int_0^1 \left[\frac{\partial}{\partial\xi}\left(\theta\frac{\partial\psi}{\partial\xi}\right) + \frac{\partial}{\partial y}\left(-\theta\frac{\partial\psi}{\partial\xi} - \frac{\partial\theta}{\partial y}\right)\right] dy = 0 \tag{3.17}$$

By changing the order of integration and differentiation and applying the Leibnitz's rule in the first, two expressions respectively on the left side, Eq. (3.17) can be rewritten as

$$\frac{\partial}{\partial \xi}\int_0^1 \theta \frac{\partial \psi}{\partial \eta}\, d\eta = \frac{\partial}{\partial \eta}\int_0^1 \left(\theta \frac{\partial \psi}{\partial \xi} + \frac{\partial \theta}{\partial \eta}\right) d\eta \tag{3.18}$$

The left side is ingetrated by parts and we then have

$$\frac{\partial}{\partial \xi}\left(\theta\psi\Big|_0^1 - \int_0^1 \psi \frac{\partial \theta}{\partial \eta}\, d\eta\right) = \left(\theta \frac{\partial \psi}{\partial \xi}\Big|_0^1 + \frac{\partial \theta}{\partial \eta}\Big|_0^1\right) \tag{3.19}$$

Applying the boundary conditions (2.9b) for ψ, Eq. (3.19) becomes

$$-\frac{\partial}{\partial \xi}\int_0^1 \psi \frac{\partial \theta}{\partial \eta}\, d\eta = \frac{\partial \theta}{\partial \eta}\Big|_0^1 \tag{3.20}$$

For adiabatic horizontal boundaries or for the equal heat flux at both upper and lower horizontal boundaries, i.e., for

$$\frac{\partial \theta}{\partial \eta}\Big|_{\eta=1} = \frac{\partial \theta}{\partial \eta}\Big|_{\eta=0}, \tag{3.21}$$

$$\frac{\partial}{\partial \xi}\int_0^1 \psi \frac{\partial \theta}{\partial \eta}\, d\eta = 0 \tag{3.22}$$

or

$$\int_0^1 \left(\frac{\partial \psi}{\partial \xi}\frac{\partial \theta}{\partial \eta} + \psi \frac{\partial^2 \theta}{\partial \xi \partial \eta}\right) = 0 \tag{3.23}$$

The situations for which either Eq. (3.22) or Eq. (3.23) can

be satisfied are examined in Appendix A. From the considerations made therein, it is shown that the only possible configuration is that the temperature distribution in the core is linear and stratified, while the core flow pattern is still parallel, i.e., θ and ψ are represented as

$$\theta = K_3 \zeta + g(y) \tag{3.24}$$

and

$$\psi = K_3 h(y) \tag{3.25}$$

where k_3 is an arbitrary constant and g(y) is an arbitrary function of y.

Substitution of (3.24) and (3.25) into Eqs. (3.7) and (3.8) yields

$$h^{iv}(y) = 1 \tag{3.26}$$

and from the boundary condition (2.9b), h(y) can then be represented as

$$h(y) = \frac{1}{24} y^2 (y-1)^2 \tag{3.27}$$

[2] $\underline{Gr_H A^2 \sim 1,\ A^2 \ll 1}$

Under this condition, the core flow equations (3.4) ~

(3.6) reduce to

$$\frac{\partial(\xi,\psi)}{\partial(x,y)} = \frac{\partial\theta}{\partial x} + \frac{\partial^2\xi}{\partial y^2} \tag{3.28}$$

$$\xi = -\frac{\partial^2\psi}{\partial y^2} \tag{3.29}$$

$$Pr\,Gr_H A^2 \frac{\partial(\theta,\psi)}{\partial(x,y)} = \frac{\partial^2\theta}{\partial y^2} \tag{3.30}$$

As in the preceding analysis, the flow characteristics are being examined according to Pr.

(i) $Pr \ll 1 \rightarrow Ra_H A^2 \ll 1$

When Pr is very small such that $Ra_H A^2 \ll 1$, from Eq. (3.9)

$$0 = \frac{\partial^2\theta}{\partial y^2} \tag{3.31}$$

This equation is identical to Eq. (3.10) which was previously treated. Referring the result in (3.12), θ can be represented as

$$\theta = K_1 x + K_2 \tag{3.32}$$

By the same reasoning as in the case (ii) of the preceding analysis, if we rewrite and integrate Eq. (3.28) over y from 0 to 1 we have

$$\frac{\partial}{\partial x}\int_0^1 \xi\frac{\partial\psi}{\partial y}dy + \frac{\partial}{\partial y}\int_0^1 (-\xi\frac{\partial\psi}{\partial x} - \frac{\partial\xi}{\partial y})dy = \int_0^1 \frac{\partial\theta}{\partial x}dy \tag{3.33}$$

Integrating the first expression on the left side by parts,

$$\frac{\partial}{\partial \xi}\left(\xi\psi\Big|_0^1 - \int_0^1 \psi \frac{\partial \xi}{\partial y}\,dy\right) - \left(\xi \frac{\partial \psi}{\partial \xi}\Big|_0^1 + \frac{\partial \xi}{\partial y}\Big|_0^1\right) = \int_0^1 \frac{\partial \theta}{\partial \xi}\,dy \qquad (3.34)$$

Substituting Eq. (3.8) into Eq. (3.34) and applying the boundary conditions (2.9b) for ψ, we then have

$$\frac{\partial}{\partial \xi}\int_0^1 \psi \frac{\partial^3 \psi}{\partial y^3}\,dy + \frac{\partial^3 \psi}{\partial y^3}\Big|_0^1 = \int_0^1 \frac{\partial \theta}{\partial \xi}\,dy \qquad (3.35)$$

Since the flow characteristics contained in Eq. (3.35) are not readily perceivable, we attempt to obtain information by examining the dependence of ψ on the arguements ζ and y in Eq. (3.35).

Considering the boundary conditions (2.9b), ζ can be represented as

$$\psi(\xi, y) = h(\xi)\, g(y) \qquad (3.36)$$

From the symmetry property of ψ in (2.10a), we have

$$h(\xi) = h(1-\xi) \qquad (3.37a)$$

and

$$g(y) = g(1-y) \qquad (3.37b)$$

Substitution of (3.32) and (3.36) into Eq. (3.35) yields

$$\frac{\partial}{\partial \xi}\int_0^1 [h(\xi)]^2 g(y) g'''(y)\,dy + h(\xi)\left[g'''(y)\Big|_0^1\right] = K_1 \qquad (3.38)$$

Carrying out the differentiation in the first expression on the left side, we find

$$2h(\xi)h'(\xi)\int_0^1 g(y)g'''(y)\,dy + h(\xi)\left[g'''(y)\Big|_0^1\right] = K_1 \qquad (3.39)$$

In Eq. (3.39), considering the boundary conditions and the symmetry property of ψ in (2.9b) and (3.37), the function g(y) is an even function about the point $y = \frac{1}{2}$. The derivative $g'''(y)$ is an odd function about $y = \frac{1}{2}$, and thus the product, $g(y)g'''(y)$, becomes an odd function about $y = \frac{1}{2}$. Then the integral $\int_0^1 g(y)g'''(y)\,dy$ becomes zero and Eq. (3.39) reduced to

$$h(\xi)\left[g'''(y)\Big|_0^1\right] = K_1 \qquad (3.40)$$

Thus

$$h(\xi) = \frac{-2g'''(0)}{K_1} = \text{const.} = K_4 \qquad (3.41)$$

Then from (3.36) and (3.41), we have

$$\psi = K_4 g(y) \qquad (3.42)$$

Substituting (3.32) and (3.42) into Eqs. (3.28) and (3.29), from the boundary conditions (2.9b) g(y) can be represented as

$$g(y) = \frac{K_1}{K_4}\frac{1}{24}y^2(y-1)^2 \qquad (3.43)$$

It is thus seen from (3.32) and (3.42) that the core flow pattern is parallel and the core temperature distribution is linear.

(ii) $\underline{Pr \sim 1 \rightarrow Ra_H A^2 \sim 1}$

When Pr is of order 1 such that $Ra_H A^2 \sim 1$, Eq. (3.9) can be written as

$$\frac{\partial(\theta,\psi)}{\partial(\zeta,y)} = \frac{\partial^2\theta}{\partial y^2} \tag{3.44}$$

This equation is identical to Eq. (3.15) which was previously treated. Referring the results indicated in Appendix B, ψ and θ can be represented as

$$\psi = \psi(y) \tag{3.45}$$

$$\theta = f(\zeta) + g(y) \tag{3.46}$$

Substitution of (3.45) and (3.46) into Eqs. (3.28) and (3.29) yields

$$f'(\zeta) = \psi^{iv}(y) = K_4 \tag{3.47}$$

where k_4 is an arbitrary constant.

From (3.46) and (3.47), θ is represented as

$$\theta = K_4\zeta + g(y) \tag{3.48}$$

From (3.47) and the boundary conditions (2.9b), ψ then becomes

$$\psi = \frac{K_4}{24} y^2(y-1)^2 \tag{3.49}$$

Thus from (3.48) and (3.49), it is seen that the core flow pattern is still parallel in this case while the core temperature distribution is linear and stratified. These are the same results as those in the case (ii) of the preceding analysis for $Gr_H A^2 \ll 1$, $Ra_H A^2 \sim 1$.

(iii) $Pr \gg 1 \rightarrow Ra_H A^2 \gg 1$

In this situation, from Eq. (3.6), heat transfer by conduction is negligible and convection is dominant in the core. Conduction of heat from the hot wall will thus be transferred by convection across the cavity to the opposite end. This implies the existence of thermal boundary layers in the end region within which most of the temperature drop occurs and there no longer exists driving force in the core. Instead the driving force will come out from the end region. For the analysis of this flow regime, different scalings based on the proper balances in the end region are needed. This situation will be considered as Case III.

[3] $Gr_H A^2 \gg 1$, $A^2 \ll 1$

In this situation, from Eq. (3.4) inertia becomes dominant in the core. Thus the balance made between buoyancy and viscous forces in the core becomes inappropriate to this situation. The flow inertia can be produced either by the driving force in the end region or by the driving force in the core. The former case will

be considered as Case III and the latter case will be considered as Case II. The explicit conditions for each situation will be delineated in the course of analysis.

3.1.3 Determination of Stretching Parameter ε_x

In the preceding analysis, it was shown that the temperature distribution in the core is either linear or linear and stratified and its flow pattern in the core is parallel. In such a flow regime, the driving force for the core flow results from the linear temperature gradients in the core and the end region is supposed to have little effect on the core flow except simply to turn the core flow to conserve the mass. Thus the proper force balance in the end region that is needed to determine ε_x would be that between the viscous diffusion along the end walls and that along the horizontal boundaries. From Eq. (2.13), this balance can be represented as

$$\frac{A^2}{\varepsilon_x^2} \sim 1 \tag{3.50}$$

and thus, $$\varepsilon_x \sim A \tag{3.51}$$

From Eq. (2.11), the variable x in the end region is of order $O(\frac{\delta_x}{L})$ and it must be stretched to make η of unit order of magnitude by means of the stretching parameter, ε_x, so that

$$\varepsilon_x \sim O\left(\frac{\delta_x}{L}\right) \tag{3.52}$$

Then, from (3.51) and (3.52), the end region characteristic length δ_x becomes of order

$$\delta_x \sim \varepsilon_x \cdot L \sim H \tag{3.53}$$

Substitution of (3.51) and (3.3) into Eqs. (2.13) ∿ (3.15) yields

$$Gr_H A^4 \frac{\partial(\xi,\psi)}{\partial(\eta,y)} + Gr_H A^3 \frac{\partial(\xi,\psi)}{\partial(\xi,y)} = \frac{\partial\theta}{\partial\eta} + A\frac{\partial\theta}{\partial\xi} + A\frac{\partial^2\xi}{\partial\eta^2} + 2A^2\frac{\partial^2\xi}{\partial\eta\partial\xi} + A^3\frac{\partial^2\xi}{\partial\xi^2} + A\frac{\partial^2\xi}{\partial y^2} \tag{3.54}$$

$$\xi = -\left(\frac{\partial^2\psi}{\partial\eta^2} + 2A\frac{\partial^2\psi}{\partial\eta\partial\xi} + A^2\frac{\partial^2\psi}{\partial\xi^2} + \frac{\partial^2\psi}{\partial y^2}\right) \tag{3.55}$$

$$Pr\,Gr_H A^3 \frac{\partial(\theta,\psi)}{\partial(\eta,y)} + Pr\,Gr_H A^3 \frac{\partial(\theta,\psi)}{\partial(\xi,y)} = A\frac{\partial^2\theta}{\partial\eta^2} + 2A^2\frac{\partial^2\theta}{\partial\eta\partial\xi} + A^3\frac{\partial^2\theta}{\partial\xi^2} + A\frac{\partial^2\theta}{\partial y^2} \tag{3.56}$$

Considering the terms with η and y derivatives in the Eqs. (3.54) ∿ (3.56), the equations which will describe the end flow characteristics can be extracted. Before doing that, one thing that should be noted is that in Eq. (3.54), by a coordinate stretching with a small parameter A, the buoyancy term in the end region, $\frac{1}{A}\frac{\partial\theta}{\partial\eta}$, becomes dominant relative to the core buoyance term, $\frac{\partial\eta}{\partial\zeta}$, which provides the driving force to the core flow. Physically this is unreasonable. This is actually due to the fact that the temperature difference in the end region, which is a small part of the total temperature change ΔT, is not properly normalized by a simple stretching of the independent variable x. This is one of the difficulties encountered due to the coupling of the governing

equations, because in the coupled equations such as Eqs. (2.13) and (2.15) herein, the two dependent variables θ and ξ do not behave similarly in the region of non-uniformity, and thus the stretching parameter, ε_x, which is determined from the consideration of either one dependent variable, does not normalize the terms with the other variable properly in the region of non-uniformity. Some modification, therefore, should be made to yield the proper normalization of the relevant equations if necessary.

In Eq. (3.54), if we separate the temperature distribution into two parts as

$$\theta(\eta, \zeta, y) = \theta_e(\eta, y) + \theta_c(\zeta, y) \tag{3.57}$$

where the subscripts c and e represent the core and end region, respectively, since

$$\theta = \frac{(T-T_c)}{\Delta T} \sim \frac{\Delta T}{\Delta T} \sim 1 \tag{3.58}$$

and

$$\theta_e = \frac{(T-T_c)_e}{\Delta T} \sim \frac{A\Delta T}{\Delta T} \sim A \tag{3.59}$$

we find

$$\frac{\partial \theta_e}{\partial \eta} \sim A \frac{\partial \theta}{\partial \eta} \tag{3.60}$$

Thus, for the proper normalization of the end region buoyancy term, we replace $\frac{\partial \theta}{\partial \eta}$ by $A \frac{\partial \theta}{\partial \eta}$ in Eq. (3.54).

Then, considering the terms with η and y derivatives, the end region flow equations can be written as

$$Gr_H A \frac{\partial(\xi,\psi)}{\partial(\eta,y)} = \frac{\partial\theta}{\partial\eta} + \frac{\partial^2\xi}{\partial\eta^2} + \frac{\partial^2\xi}{\partial y^2} \tag{3.61}$$

$$\xi = -\left(\frac{\partial^2\psi}{\partial\eta^2} + \frac{\partial^2\psi}{\partial y^2}\right) \tag{3.62}$$

$$Pr\, Gr_H A \frac{\partial(\theta,\psi)}{\partial(\eta,y)} = \frac{\partial^2\theta}{\partial\eta^2} + \frac{\partial^2\theta}{\partial y^2} \tag{3.63}$$

The method of multiple scales has yielded Eqs. (3.54) ∿ (3.56) which indicate explicitly what equations are applicable in each region and in the interaction region. From those equations, two sets of equations, one for the core flow and the other for the end region flow, are extracted. Eqs. (3.4) ∿ (3.6) for the core flow and Eqs. (3.61) ∿ (3.63) for the end region flow are identical to those obtained by Cormack et. al. [27] for $A \to 0$, Gr_H fixed while present equations are valid for $A^2 \ll 1$, $Gr_H A^2 \lesssim 1$ and $Ra_H A^2 \lesssim 1$. However, the buoyancy term was not properly normalized in [27] so that the coefficient in their equations differ from that in Eq. (3.61). It should be noted that the buoyancy does contribute to the flow in the end region in contradistinction to the description given by Cormack et. al.

Since our primary concern herein is general flow patterns based on the core configurations, no attempt will be made to obtain the solution of the basic equations at this time.

CASE II: Balance between Buoyancy and Inertia Forces in the Core

3.2.1 Basic Equations

In Case I, the analysis was made based on the balance between buoyancy and viscous forces in the core. The balance made therein was shown to be inappropriate when $Gr_H A^2 >> 1$, because the inertia becomes dominant in the core under that condition. We now study the flow characteristics considering the balance between buoyancy and inertia forces in the core.

From Eq. (2.13), the balance between buoyancy and inertia forces in the core can be represented as

$$\frac{\beta g \Delta T_c^2 H}{v_R^2} \sim 1 \tag{3.64}$$

Specifying ΔT_c as H by the same reasoning in (3.2), v_R becomes

$$v_R \sim (\beta g \Delta T H^3)^{\frac{1}{2}} \tag{3.65}$$

Here we also leave the determination of the stretching parameter, ε_x, to later, after studying the core flow characteristics.

Substituting (3.65) into Eqs. (2.13) ~ (2.15) and considering the terms with ζ and y derivatives, the core flow equations can be written as

$$\frac{\partial(\xi,\psi)}{\partial(\zeta,y)} = \frac{\partial\theta}{\partial\zeta} + \frac{1}{\sqrt{Gr_H}A^2}\left(A^2\frac{\partial^2\xi}{\partial\zeta^2} + \frac{\partial^2\xi}{\partial y^2}\right) \tag{3.66}$$

$$\xi = -\left(A^2 \frac{\partial^2 \psi}{\partial \zeta^2} + \frac{\partial^2 \psi}{\partial y^2} \right) \tag{3.67}$$

$$\frac{\partial(\theta, \psi)}{\partial(\zeta, y)} = \frac{1}{\sqrt{Pr\,Ra_H\, A^2}} \left(A^2 \frac{\partial^2 \theta}{\partial \zeta^2} + \frac{\partial^2 \theta}{\partial y^2} \right) \tag{3.68}$$

For the situation $Gr_H A^2 >> 1$ concerned herein, Pr appears as a parameter in Eq. (3.68). Because consideration is being given to the situation in which the driving force exists in the core, the analysis will be valid within the parameteric range of $PrRa_H A^2 \lesssim 1$ which is possible only for $Pr^2 \lesssim \frac{1}{Gr_H A^2}$, i.e., for low Pr. But it will be shown later in the analysis that the validity of analysis is confined to the parametric range of $Gr_H A^2 \gg 1$, $Pr^2 \ll \frac{1}{Gr_H A^2}$ so that $PrRa_H A^2 << 1$. In addition, one thing to be noted is that for $Gr_H A^2 >> 1$, viscous diffusion terms would seem to be negligible compared to the other terms in Eq. (3.66). However, since these terms are the derivatives of the highest order in the equations, Eq. (3.66) is singular and this implies that for negligible horizontal diffusion term, $A^2 \frac{\partial^2 \xi}{\partial \zeta^2}$, in the core for $A^2 << 1$, there exists a thin layer very near the horizontal boundaries within which the vertical viscous diffusion term, $\frac{\partial^2 \xi}{\partial y^2}$, is important. The effect of viscous diffusion is not regarded to be so large as to affect the core flow structure in this inertia important flow regime concerned herein.

3.2.2 Core Flow Characteristics

For $Gr_H A^2 \gg 1$, Eq. (3.66) reduces to

$$\frac{\partial(\xi,\psi)}{\partial(\xi,\eta)} = \frac{\partial\theta}{\partial\xi} \tag{3.69}$$

For $Pr^2 \lesssim \frac{1}{Gr_H A^2}$, $PrRa_H A^2$ acts as a parameter in Eq. (3.68). We thus examine the core configurations according to this parameter.

(i) $PrRa_H A^2 \ll 1$, $\cdots \ll 1$

When $Pr^2 \ll \frac{\cdot}{Gr_H A^2}$, i.e., Pr is very small so that $PrRa_H A^2 \ll 1$, Eq. (3.18) reduces to

$$0 = \frac{\partial^2\theta}{\partial\eta^2} \tag{3.70}$$

This equation is identical to Eqs. (3.10) and (3.31) which were previously treated. Referring the result in (3.18), θ can be represented as

$$\theta = K_1\xi + K_2 \tag{3.71}$$

Then, from Eq. (3.19) and (3.71)

$$\frac{\partial(\xi,\psi)}{\partial(\xi,\eta)} = K_1 = const. \tag{3.72}$$

In order that Eq. (3.72) is valid, ψ should be a function of both variables as

$$\psi = \psi(\xi,\eta) \tag{3.73}$$

This implies that the core flow pattern becomes non-parallel when the inertia is important in the core, although the flow is driven by the buoyancy force in the core.

(ii) $\underline{Pr Ra_H A^2 \sim 1,\ A^2 \ll 1}$

In this case, Eq. (3.68) reduces to

$$\frac{\partial(\theta,\psi)}{\partial(\zeta,\eta)} = \frac{\partial^2\theta}{\partial\eta^2} \tag{3.74}$$

This equation is identical to Eq. (3.15) in Case I which was previously treated. Following the same procedure in Case I, for adiabatic horizontal boundaries, from Eqs. (3.22) and (3.23) we have

$$\frac{\partial}{\partial\zeta}\int_0^1 \psi\,\frac{\partial\theta}{\partial\eta} = 0 \tag{3.75}$$

or

$$\int_0^1 \left(\frac{\partial\psi}{\partial\zeta}\frac{\partial\theta}{\partial\eta} + \psi\frac{\partial^2\theta}{\partial\zeta\partial\eta}\right) d\eta = 0 \tag{3.76}$$

The situations for which either Eq. (3.75) or (3.76) can be satisfied are examined in Appendix B. From the considerations made therein, it was found that the driving force for this case could not occur in the core. Thus, in this situation the balance based on the driving force in the core is inappropriate and the analysis based on that balance will be valid only for $Pr Ra_H A^2 \ll 1$. Actually for $Pr^2 \ll \frac{1}{Gr_H A^2}$ (i.e., for $Pr \ll 1$), the condition $Pr Ra_H A^2 \sim 1$ is possible only when $Ra_H A^2 \gg 1$ in which case the driving force was mentioned to exist in the end region in Case I.

This situation will, therefore, be considered as Case III.

(iii) $PrRa_H A^2 >> 1$

In this case, convection becomes dominant in the core in Eq. (3.68), thus there no longer exists the driving force in the core. This is also the case of $Ra_H A^2 >> 1$ and will be considered as Case III.

3.2.3 Determination of ε_x

In the above, although the core flow is driven by the buoyancy force in the core, the core flow pattern was shown to be non-parallel. In this situation, the proper force balance for the end region, from which the stretching parameter, ε_x, is also determined, is not readily apparent. However, considering the relative dominance of inertia with respect to viscous friction in the core and the consequent non-parallel core flow structure, two possible mechanisms can be inferred: The first one is that the inertia in the end region can be as influential on the core flow structure as the inertia in the core. The second one is that the inertia in the core can be damped by the viscous diffusion in the end. Based on these two inferrences, we thus make the corresponding force balances for the end region and to see what the results would imply.

For the first situation, the balance between the inertia in the end and the inertia in the core is appropriate. From Eq. (2.13),

this balance can be represented as

$$\frac{1}{\varepsilon_x} \sim 1 \tag{3.77}$$

Thus, $$\varepsilon_x \sim 1 \tag{3.78}$$

From (3.52) and (3.78), δ_x becomes of order

$$\delta_x \sim \varepsilon_x \cdot L \sim L \tag{3.79}$$

This tells us that there is no difference in horizontal length scale between the core and end region, which means that no clear distinction could be made between the two regions. In addition, since $\varepsilon_x \sim 1$, there is no distinction between the equations with the variables (η, y) and (ζ, y), i.e., in the end and core regions. The core flow picture in this situation will thus be valid throughout the whole cavity except the very thin layer adjacent to the solid boundaries which is supposed to exist due to the singular behaviour of the viscous diffusion terms for $Gr_H A^2 >> 1$ in Eq. (3.66). Consequently the vertical flow (or turning flow) in the cavity is not necessarily confined to the region near the end walls in this case as in the case of parallel core flow. Instead it may spread over the entire configuration.

For the second situation, the balance between the viscous diffusion in the end and the inertia in the core is appropriate. From Eq. (2.13), this balance can be represented as

$$\frac{\nu L}{\Psi_R H} \frac{A^2}{\varepsilon_x^2} \sim 1 \tag{3.80}$$

From (3.65) and (3.80), ε_x becomes

$$\varepsilon_x \sim \frac{A}{(Gr_H A^2)^{\frac{1}{4}}} \tag{3.81}$$

From (3.52), δ_x then becomes of order

$$\delta_x \sim \frac{H}{(Gr_H A^2)^{\frac{1}{4}}} \tag{3.82}$$

Since $Gr_H A^2 >> 1$

$$\frac{\delta_x}{H} < 1 \tag{3.83}$$

Substituting (3.65) and (3.81) into Eqs. (2.13) ~ (2.15) and considering the terms with η and y derivatives, the end flow equations can be extracted. However, in this situation the end region buoyancy term, $\frac{1}{\varepsilon_x}\frac{\partial\theta}{\partial\eta}$, which is of order

$$\frac{1}{\varepsilon_x}\frac{\partial\theta}{\partial\eta} \sim \frac{(Gr_H A^2)^{\frac{1}{4}}}{A}\frac{\partial\theta}{\partial\eta} \tag{3.84}$$

becomes dominant relative to the core buoyancy term, $\frac{\partial\theta}{\partial\zeta}$.

As in the analysis of Case I, even though we renormalize the end region buoyancy term with $A\Delta T$, the proper end region characteristic temperature difference, the modified end region buoyancy term, $(Gr_H A^2)^{\frac{1}{4}}\frac{\partial\theta}{\partial\eta}$, still becomes greater than that in the core for the condition $Gr_H A^2 >> 1$ herein. This implies that temperature drops greater than $A\Delta T$ occurs in the end region, and that will be possible when rather steeper non-linear temperature gradient exists in the end. In this case, considering the fact that $\frac{\delta_x}{H} < 1$ in (3.83), the core flow will be rather driven by the buoyancy in the end region

than by the buoyancy in the core. Thus, this second case appears a much less plausible situation than the first one.

CASE III: Balance between Convection and Conduction in the End Region

In the previous analysis of Cases I and II, situations were considered in which the driving force exists in the core and the approximate criteria were given therein within which each analysis is valid. Beyond such criteria, i.e., for $Ra_H A^2 >> 1$, convection becomes dominant and the diffusion of heat is negligible in the core, thus most of the temperature drop (or increase) will occur in the end region and will be convected across the cavity to the opposite end. This implies the existence of thermal boundary layer in the end region within which most of the temperature drop (or increase) occurs. It also implies the existence of thermal boundary layer structure along the horizontal boundaries in the core through which the heat will be convected to the opposite end. There thus exists no driving force in the core, instead it will come from the end region. In what follows, consideration is given to this situation according to Pr, because physically for different Pr, different force balances need to be made.

3.3.1 Pr $\gtrsim$ 1 (including Pr >> 1)

3.3.1.1 Basic Equations

For the situation mentioned above, the heat transfer between the two end walls is dominated by convection. Heat transfer by

conduction is assumed to be important only in thin boundary layers adjacent to the end walls. We thus balance the convection and conduction in the end region. In addition, since all the buoyancy force acts within the thermal boundary layers in the end region and the viscous effects are important therein for $Pr \gtrsim 1$ (including $Pr >> 1$) because the flow boundary layers extend beyond the thermal boundary layers for large Pr, we also balance the buoyancy and viscous forces in the end region, by means of which the stretching parameter, ε_x, can be determined.

From Eq. (2.15), the balance between convection and conduction in the end region can be represented as

$$\frac{1}{\varepsilon_x} \sim \frac{\alpha L}{\Psi_R H} \frac{A^2}{\varepsilon_x^2} \tag{3.85}$$

From Eq. (2.13), the balance between buoyancy and viscous forces in the end region can be represented as

$$\frac{\beta g \Delta T \ell^2 H}{\Psi_R^2} \frac{1}{\varepsilon_x} \sim \frac{\nu L}{\Psi_R H} \frac{A^2}{\varepsilon_x^2} \tag{3.86}$$

Considering that the flow is driven by the buoyancy force in the end region, the vorticity would be dominant therein. It is thus appropriate to represent the characteristic vorticity, Ξ_R, by specifying the characteristic length ℓ as δ_x, as

$$\ell \sim \delta_x \tag{3.87}$$

and $$\Xi_R \sim \frac{\psi_R}{\delta_x^2} \tag{3.88}$$

From (3.85) ~ (3.87), we then obtain

$$\psi_R \sim \alpha Ra_H^{\frac{1}{4}} \tag{3.89}$$

and $$\varepsilon_x \sim \frac{A}{Ra_H^{\frac{1}{4}}} \tag{3.90}$$

From (3.52) and (3.90), we find

$$\delta_x \sim \frac{H}{Ra_H^{\frac{1}{4}}} \tag{3.91}$$

In (3.91), it is seen that the end region characteristic length δ_x is similar to the familiar thermal boundary layer thickness of a vertical flat plate.

Substitution of ψ_R, ε_x and δ_x into Eqs. (2.13) ~ (2.15) then yields

$$\frac{Ra_H^{\frac{1}{4}}}{A}\frac{\partial(\Xi,\psi)}{\partial(\eta,\gamma)} + \frac{\partial(\Xi,\psi)}{\partial(\zeta,\gamma)} = Pr\cdot\left(\frac{Ra_H^{\frac{1}{4}}}{A}\frac{\partial\theta}{\partial\eta} + \frac{\partial\theta}{\partial\zeta}\right) + Pr\cdot\left(\frac{Ra_H^{\frac{1}{4}}}{A}\frac{\partial^2\Xi}{\partial\eta^2} + 2\frac{\partial^2\Xi}{\partial\eta\partial\zeta} + \frac{A}{Ra_H^{\frac{1}{4}}}\frac{\partial^2\Xi}{\partial\zeta^2} + \frac{1}{A\,Ra_H^{\frac{1}{4}}}\frac{\partial^2\Xi}{\partial\gamma^2}\right) \tag{3.92}$$

$$\Xi = -\left(\frac{\partial^2\psi}{\partial\eta^2} + \frac{2A}{Ra_H^{\frac{1}{2}}}\frac{\partial^2\psi}{\partial\eta\partial\zeta} + \frac{A^2}{Ra_H^{\frac{1}{2}}}\frac{\partial^2\psi}{\partial\zeta^2} + \frac{1}{Ra_H^{\frac{1}{2}}}\frac{\partial^2\psi}{\partial\gamma^2}\right) \tag{3.93}$$

$$\frac{Ra_H^{\frac{1}{4}}}{A}\frac{\partial(\theta,\psi)}{\partial(\eta,\gamma)} + \frac{\partial(\theta,\psi)}{\partial(\zeta,\gamma)} = \frac{Ra_H^{\frac{1}{4}}}{A}\frac{\partial^2\theta}{\partial\eta^2} + 2\frac{\partial^2\theta}{\partial\eta\partial\zeta} + \frac{A}{Ra_H^{\frac{1}{4}}}\frac{\partial^2\theta}{\partial\zeta^2} + \frac{1}{A\,Ra_H^{\frac{1}{4}}}\frac{\partial^2\theta}{\partial\gamma^2} \tag{3.94}$$

Considering the terms of η and γ derivatives in Eqs. (3.92) ~ (3.94), the equations for the end region flow can be extracted as

$$\frac{1}{Pr}\frac{\partial(\xi,\psi)}{\partial(\eta,y)} = \frac{\partial\theta}{\partial\eta} + \frac{\partial^2\xi}{\partial\eta^2} + \frac{1}{Ra_H^{1/2}}\frac{\partial^2\xi}{\partial y^2} \tag{3.95}$$

$$\xi = -\left(\frac{\partial^2\psi}{\partial\eta^2} + \frac{1}{Ra_H^{1/2}}\frac{\partial^2\psi}{\partial y^2}\right) \tag{3.96}$$

$$\frac{\partial(\theta,\psi)}{\partial(\eta,y)} = \frac{\partial^2\theta}{\partial\eta^2} + \frac{1}{Ra_H^{1/2}}\frac{\partial^2\theta}{\partial y^2} \tag{3.97}$$

With its characteristic length δ_x in Eq. (3.91), the end region flow equations (3.95) ∿ (3.97) are similar to the boundary layer equations of a vertical flat plate. Under similar boundary conditions, the flow and heat transfer characteristics in the end region will thus be similar to those in the case of a vertical flat plate except that they are influenced by the core.

Considering the derivatives with respect to ζ and y, the equations which will describe the core flow can be written as

$$\frac{1}{Pr}\frac{\partial(\xi,\psi)}{\partial(\zeta,y)} = \frac{\partial\theta}{\partial\zeta} + \frac{1}{ARa_H^{1/2}}\left(A^2\frac{\partial^2\xi}{\partial\zeta^2} + \frac{\partial^2\xi}{\partial y^2}\right) \tag{3.98}$$

$$\xi = -\frac{1}{Ra_H^{1/2}}\left(A^2\frac{\partial^2\psi}{\partial\zeta^2} + \frac{\partial^2\psi}{\partial y^2}\right) \tag{3.99}$$

$$\frac{\partial(\theta,\psi)}{\partial(\zeta,y)} = \frac{1}{ARa_H^{1/2}}\left(A^2\frac{\partial^2\theta}{\partial\zeta^2} + \frac{\partial^2\theta}{\partial y^2}\right) \tag{3.100}$$

Let us look at the core flow characteristics based on the di-

mensionless parameters in the Eqs. (3.98) ∿ (3.100).

3.3.1.2 Core Flow Characteristics

[1] $\frac{1}{ARa_H^{\frac{1}{4}}} < 1,\ A^2 << 1$

In Eq. (3.100), when $\frac{1}{ARa_H^{\frac{1}{4}}} < 1$ (or $ARa_H^{\frac{1}{4}} > 1$) the conduction terms are negligible compared to the convection terms. But as these terms are the derivatives of the highest order in the equation, for negligible horizontal conduction term the equation is singular with respect to y in the core. This implies that there exists a thin layer (it is called here "horizontal thermal layer") adjacent to the horizontal boundaries within which the vertical conduction term becomes important. This horizontal layer can be estimated by the coordinate stretching method. For the consideration of the horizontal thermal layer we thus introduce the transformation as

$$y = \varepsilon_y \tilde{y} \tag{3.101}$$

where

$$\varepsilon_y \sim \frac{\delta_y}{H} \tag{3.102}$$

and δ_y represent the horizontal thermal layer.

Substituting the derivatives of (3.101) into Eq. (3.100) and balancing the convection and conduction within δ_y, we then have

$$\frac{1}{\varepsilon_y} \sim \frac{1}{ARa_H^{\frac{1}{4}}} \quad \frac{1}{\varepsilon_y^2} \tag{3.103}$$

From (3.102) and (3.103), we find

$$\delta_y \sim \frac{L}{Ra_H^{\frac{1}{4}}} \tag{3.104}$$

or $$\frac{\delta_y}{H} \sim \frac{1}{ARa_H^{\frac{1}{4}}} \tag{3.105}$$

In order that the horizontal thermal layer be distinct,

$$\frac{\delta_y}{H} < 1 \tag{3.106}$$

so that $$ARa_H^{\frac{1}{4}} > 1 \tag{3.107}$$

Under the condition (3.107), to a good approximation, the core flow equation (3.98) and (3.100) reduce to

$$\frac{1}{Pr}\frac{\partial(\xi,\psi)}{\partial(\zeta,\gamma)} = \frac{\partial\theta}{\partial\zeta} \tag{3.108}$$

$$\frac{\partial(\theta,\psi)}{\partial(\zeta,\gamma)} = 0 \tag{3.109}$$

Eqs. (3.108) and (3.109) will thus describe the core configuration outside the horizontal thermal layer, i.e., in the mid-core region, under the condition (3.107). Since Pr acts as a parameter in Eq. (3.108), we first examine the core flow characteristics for high Pr ($Pr \gg 1$) and then for moderate Pr ($Pr \sim 1$).

(i) <u>$Pr \gg 1$</u>

For $Pr \gg 1$, the inertia term in Eq. (3.108) becomes negligible

and we have

$$\frac{\partial \theta}{\partial \zeta} = 0 \tag{3.110}$$

From (3.110), two possible temperature profiles can be obtained as

$$\theta_c = \theta_c(y) \tag{3.111}$$

or $$\theta_c = \text{const.} \tag{3.112}$$

where the subscript c is affixed to denote the temperature distribution outside the horizontal thermal layer. Among the two possible core configurations, it is shown in Appendix C that the case θ_c = const. is inappropriate to the situation concerned herein.

From (3.109) and (3.111), we find

$$\frac{\partial \psi}{\partial \zeta} = 0 \tag{3.113}$$

and $$\psi = \psi(y) \tag{3.114}$$

From (3.111) and (3.114), it therefore can be seen that for Pr >> 1, under the condition $AR a_H^{\frac{1}{4}} > 1$ there exists the horizontal thermal layer in the core and the temperature distribution outside the horizontal thermal layer, i.e., in the mid-core, will be stratified while the corresponding core flow structure will be parallel. This parallel core flow structure was observed in the experiment of Ostrach et. al. [31] for Pr = 1.38×10^3, A = 0.1 and $Ra_H \sim 10^6$, but the horizontal walls are semi-conducting therein.

(ii) <u>Pr ~ 1</u>

When $Pr \sim 1$, (in fact Pr is about 1 or slightly greater than 1), the inertia term in Eq. (3.108) is not negligible. Instead the circulating flow will transport vorticity across the cavity by the inertia and, as can be conceivable by the singular behaviour in the equation, the diffusion of vorticity will be important within a layer (we call it here "horizontal viscous layer" in distinction to the horizontal thermal layer) along the horizontal boundaries. This horizontal viscous layer can be estimated form the balance between the vorticity transport and diffusion terms within that layer. But in this case, we have to use a modified characteristic stream function $\bar{\Psi}_R$ instead of Ψ_R , because the characteristic stream function has different values according to the different characteristic length scales within which difference balances are made. In Appendix D, the modified characteristic stream function $\bar{\Psi}_R$ is estimated. The argument of the necessity of the distinction between the two characteristic stream function is also given therein.

For an estimate of the horizontal viscous layer, we introduce the transformation as

$$y = \varepsilon_v \tilde{y} \tag{3.115}$$

where

$$\varepsilon_v \sim \frac{\delta_v}{H} \tag{3.116}$$

and δ_v is the horizontal viscous layer.

Substituting the derivatives of (3.115) into Eq. (3.98) with

the modified characteristic stream function $\bar{\Psi}_R$ replaced by Ψ_R, from the balance between the vorticity transport and diffusion terms within δ_v, we have

$$\frac{1}{\epsilon_v} \sim \frac{\nu L}{\bar{\Psi}_R H} \frac{1}{\epsilon_v^2} \tag{3.117}$$

From Appendix D, as

$$\bar{\Psi}_R \sim a\, Pr^{\frac{1}{2}} Ra_H^{\frac{1}{4}} \tag{3.118}$$

from (3.116), (3.117) and (3.118), we find

$$\epsilon_v \sim \frac{Pr^{\frac{1}{2}} L}{Ra_H^{\frac{1}{4}}} \tag{3.119}$$

or
$$\frac{\epsilon_v}{H} \sim \frac{Pr^{\frac{1}{2}}}{ARa_H^{\frac{1}{4}}} \tag{3.120}$$

For distinct horizontal viscous layer,

$$\frac{\delta_v}{H} < 1 \tag{3.121}$$

so that
$$ARa_H^{\frac{1}{4}} > Pr^{\frac{1}{2}} \tag{3.122}$$

Since $Pr \sim 1$, from (3.104) and (3.119)

$$\frac{\delta_v}{\delta_y} \sim Pr^{\frac{1}{2}} \sim 1 \tag{3.123}$$

Under condition (3.122), the effect of visc us shear in the core is confined to the horizontal viscous layer, δ_v. Here, since the flow is driven by the boundary layer in the end region and there is no other way to induce any fluid motion in the core except by

the viscous shear of the end driven circulating flows. Since $\delta_v \sim \delta_y$ from (3.123), most of the flow in the core will thus circulate through the horizontal viscous layer adjacent to the horizontal boundaries. Outside that layer, the flow which may result from the entrainment-detrainment of the end driven core circulating flow would be of much lower order than the circulating flow so that the motion therein would be almost stagnant.

If we compare the order of vorticity within the horizontal viscous layer to that outside the horizontal viscous layer, from (3.121) we find

$$\frac{\xi_o}{\xi_i} = \frac{\bar{\psi}_R/H^2}{\bar{\psi}_R/\delta_v^2} = \left(\frac{\delta_v}{H}\right)^2 << 1 \tag{3.124}$$

where subscripts i and o denote the region within and outside the horizontal viscous layer, respectively.

Outside the horizontal viscous layer, we may thus put

$$\psi_c = \text{const.} \tag{3.125}$$

Then since $\delta_v \sim \delta_y$, from (3.108) we find

$$\frac{\partial \theta}{\partial \zeta} = 0 \tag{3.126}$$

and thus $$\theta_c = \theta_c(y) \tag{3.127}$$

as indicated in Appendix C.

For θ_c = const., there is no convection at all outside δ_v and the energy equation (3.109) is automatically satisfied.

From (3.125) and (3.127), it is thus seen that for Pr $\gtrsim$ 1, under the condition $ARa_H^{\frac{1}{4}} > 1$ there exists the horizontal thermal layer in the core and the temperature distribution in the mid-core will be stratified while the fluid motion therein would be almost stagnant. This stagnant core configuration was observed in the experiment of Al-Homoud [32] for Pr = 7.0, A = 0.0625 and Ra_H = $2.0 \times 10^8 \sim 2.0 \times 10^9$. This shows good agreement with the above prediction.

[2] $\dfrac{1}{ARa_H^{\frac{1}{4}}} \gtrsim 1$, $A^2 \ll 1$

Under this condition, the conduction term becomes important in Eq. (3.100) and from (3.105), the horizontal thermal layer δ_y becomes of order

$$\frac{\delta_y}{H} \sim \frac{1}{ARa_H^{\frac{1}{4}}} \gtrsim 1 \tag{3.128}$$

There thus will no longer exist distinct horizontal thermal layers in the core. Instead some horizontal temperature gradient will exist in the core which may develop fluid motion in the core in addition to the end driven circulating flow. Further it is supposed that the thermal boundary layer structure in the end region may somewhat be altered due to the core temperature gradient. Thus the resulting flow driving mechanism should be modified from the strict

end region boundary layer driven flow mechanism. The flow characteristics in this situation are, therefore, supposed to lie between those in the flow regime of Case I and in the strict boundary layer driven flow regime of Case III. In this sense this flow regime is called herein the "Intermediate Flow Regime". The condition, $ARa_H^{\frac{1}{4}} > 1$, in (3.107) would then be a necessary condition for the existence of a distinct boundary layer flow regime for $Pr \gtrsim 1$ (including $Pr >> 1$). This argument can be verified by the experimental results of Imberger [29], Al-Homoud [32] and Kamotani et. al [33].

Flow characteristics with the core configurations in the intermediate flow regime will be considered in the detailed analysis, because it is not clear here whether its characteristic length scales would be geometric length scales or not.

3.3.2 Pr < 1 *

3.3.2.1 Basic Equations

For $Pr < 1$, the flow boundary layer extends less than the thermal boundary layer and the main body of fluid can be considered to be inviscid within the thermal boundary layer except in the vicinity of end walls. Since all the buoyancy force acts within the thermal boundary layer, in addition to the balance between convection and conduction in the end region, we also balance the buoyancy and inertia forces in the end region from which the stretching parameter,

* This always includes the case of $Pr << 1$

ε_x, can be determined.

From Eq. (2.13), the balance between buoyancy and inertia forces in the end region can be represented as

$$\frac{1}{\varepsilon_x} \sim \frac{\beta g \Delta T H^2}{\nu R^2} \frac{1}{\varepsilon_x} \tag{3.129}$$

Then, with the balance between convection and conduction in the end region in (3.85), from (3.87) and (3.129) we obtain

$$\nu_R \sim \alpha (Pr Ra_H)^{\frac{1}{4}} \tag{3.130}$$

and

$$\varepsilon_x \sim \frac{A}{(Pr Ra_H)^{\frac{1}{4}}} \tag{3.131}$$

From (3.52) and (3.131), we find

$$\delta_x \sim \frac{H}{(Pr Ra_H)^{\frac{1}{4}}} \tag{3.132}$$

Substituting ν_R, ε_x and δ_x into Eqs. (2.13) $\sim$ (2.15), we then obtain

$$\frac{(Pr Ra_H)^{\frac{1}{4}}}{A} \frac{\partial(\xi,\psi)}{\partial(\eta,\zeta)} + \frac{\partial(\xi,\psi)}{\partial(\zeta,\zeta)} = \frac{(Pr Ra_H)^{\frac{1}{4}}}{A} \frac{\partial\theta}{\partial\eta} + \frac{\partial\theta}{\partial\zeta} + Pr\left[\frac{(Pr Ra_H)^{\frac{1}{4}}}{A} \frac{\partial^2\xi}{\partial\eta^2} + 2\frac{\partial^2\xi}{\partial\eta\partial\zeta} + \frac{A}{(Pr Ra_H)^{\frac{1}{4}}} \frac{\partial^2\xi}{\partial\zeta^2} + \frac{1}{A(Pr Ra_H)^{\frac{1}{4}}} \frac{\partial^2\xi}{\partial y^2}\right] \tag{3.133}$$

$$\xi = -\left[\frac{\partial^2\psi}{\partial\eta^2} + \frac{2A}{(Pr Ra_H)^{\frac{1}{4}}} \frac{\partial^2\psi}{\partial\eta\partial\zeta} + \frac{A^2}{(Pr Ra_H)^{\frac{1}{2}}} \frac{\partial^2\psi}{\partial\zeta^2} + \frac{1}{(Pr Ra_H)^{\frac{1}{2}}} \frac{\partial^2\psi}{\partial y^2}\right] \tag{3.134}$$

$$\frac{(Pr Ra_H)^{\frac{1}{4}}}{A} \frac{\partial(\theta,\psi)}{\partial(\eta,\zeta)} + \frac{\partial(\theta,\psi)}{\partial(\zeta,y)} = \frac{(Pr Ra_H)^{\frac{1}{4}}}{A} \frac{\partial^2\theta}{\partial\eta^2} + 2\frac{\partial^2\theta}{\partial\eta\partial\zeta} + \frac{A}{(Pr Ra_H)^{\frac{1}{4}}} \frac{\partial^2\theta}{\partial\zeta^2} + \frac{1}{A(Pr Ra_H)^{\frac{1}{4}}} \frac{\partial^2\theta}{\partial y^2} \tag{3.135}$$

Considering the derivatives with respect to η and y in Eqs. (3.133) $\sim$ (3.135), the end region flow equations can be represented as

$$\frac{\partial(\xi,\psi)}{\partial(\eta,y)} = \frac{\partial\theta}{\partial\eta} + Pr\cdot\left[\frac{\partial^2\xi}{\partial\eta^2} + \frac{1}{(Pr\,Ra_H)^{1/2}}\frac{\partial^2\xi}{\partial y^2}\right] \tag{3.136}$$

$$\xi = -\left[\frac{\partial^2\psi}{\partial\eta^2} + \frac{1}{(Pr\,Ra_H)^{1/2}}\frac{\partial^2\psi}{\partial y^2}\right] \tag{3.137}$$

$$\frac{\partial(\theta,\psi)}{\partial(\eta,y)} = \frac{\partial^2\theta}{\partial\eta^2} + \frac{1}{(Pr\,Ra_H)^{1/2}}\frac{\partial^2\theta}{\partial y^2} \tag{3.138}$$

With the characteristic length δ_x in Eq. (3.132), the equations (3.136) $\sim$ (3.138) are also similar to the boundary layer equations of a vertical flat plate.

Considering the derivatives with respect to ζ and y, the core flow equations can be represented as

$$\frac{\partial(\xi,\psi)}{\partial(\zeta,y)} = \frac{\partial\theta}{\partial\zeta} + \frac{Pr}{A(Pr\,Ra_H)^{1/2}}\left(A^2\frac{\partial^2\xi}{\partial\zeta^2} + \frac{\partial^2\xi}{\partial y^2}\right) \tag{3.139}$$

$$\xi = -\frac{1}{(Pr\,Ra_H)^{1/2}}\left(A^2\frac{\partial^2\psi}{\partial\zeta^2} + \frac{\partial^2\psi}{\partial y^2}\right) \tag{3.140}$$

$$\frac{\partial(\theta,\psi)}{\partial(\zeta,y)} = \frac{1}{A(Pr\,Ra_H)^{1/2}}\left(A^2\frac{\partial^2\theta}{\partial\zeta^2} + \frac{\partial^2\theta}{\partial y^2}\right) \tag{3.141}$$

In the following, we examine the core flow characteristics based on the dimensionless parameters among the core flow equations.

3.3.2.2 Core Flow Characteristics

[1] $\frac{1}{A(PrRa_H)^{\frac{1}{4}}} < 1$, $A2 \ll 1$

When $\frac{1}{A(PrRa_H)^{\frac{1}{4}}} < 1$, both the viscous and heat diffusion terms become negligible in Eqs. (3.139) and (3.144) and as in the previous analysis, the horizontal layers can be estimated by the coordinate stretching method.

Substituting the derivatives of (3.101) into Eq. (3.141) and balancing the convection and conduction within δ_y, we have

$$\frac{1}{\varepsilon_y} \sim \frac{1}{A(PrRa_H)^{\frac{1}{4}}} \frac{1}{\varepsilon_y 2} \tag{3.142}$$

From (3.102) and (3.142), we then find

$$\frac{\delta_y}{H} \sim \frac{1}{A(PrRa_H)^{\frac{1}{4}}} \tag{3.143}$$

In order that the horizontal thermal layer be distinct,

$$\frac{\delta_y}{H} < 1 \tag{3.144}$$

or $$A(PrRa_H)^{\frac{1}{4}} > 1 \tag{3.145}$$

Under the condition (3.145), to a good approximation, outside the horizontal thermal layer δ_x, i.e., in the mid-core, the core flow equaitons (3.139) and (3.141) reduce to

$$\frac{\partial(\xi,\psi)}{\partial(\zeta,\gamma)} = \frac{\partial\theta}{\partial\zeta} \tag{3.146}$$

$$\frac{\partial(\theta,\psi)}{\partial(\zeta,\gamma)} = 0 \tag{3.147}$$

For Pr < 1, as can be seen from the works of Ostrach [43] and Sparrow and Gregg [44], the thickness of velocity boundary layers along the end walls is less than (or about equal to) that of thermal boundary layers. In the core, it is also expected that the horizontal viscous layer is less than (or about equal to) the horizontal thermal layer. In this situation, as mentioned in Appendix D, the value of characteristic stream function within the horizontal thermal layer will be identical to that within the horizontal viscous layer. There thus is no need to modify the characteristic stream function for the estimation of horizontal viscous layer. Then, by introducing the transformation of (3.115) into Eq. (3.139) and from the balance between the vorticity transport and diffusion terms within the horizontal viscous layer δ_v, we find

$$\frac{\delta_v}{H} \sim \frac{Pr}{A(PrRa_H)^{\frac{1}{4}}} \tag{3.148}$$

For distinct horizontal viscous layer

$$\frac{\delta_v}{H} < 1 \tag{3.149}$$

so that $A(PrRa_H)^{\frac{1}{4}} > Pr$ (3.150)

From (3.144) and (3.148), it can be shown that

$$\delta_v < \delta_y \tag{3.151}$$

for $Pr < 1$.

Under condition (3.150), the effect of viscous shear in the core will be confined to the horizontal viscous layer and since $\delta_v < \delta_y$ in (3.151), most of the flow in the core will thus circulate through the horizontal thermal layer. Outside the horizontal thermal layer, as mentioned earlier in the previous analysis, the fluid motion would remain nearly stagnant. We may thus put

$$\psi_c = \text{const.} \tag{3.152}$$

in the mid-core region.

Then, from Eq. (3.146) we find

$$\frac{\partial \theta}{\partial \zeta} = 0 \tag{3.153}$$

and thus $\theta_c = \theta_c(y)$ (3.154)

as indicated in Appendix C.

It is thus seen from (3.152) and (3.154) that for $Pr < 1$, under the condition $A(PrRa_H)^{\frac{1}{4}} > 1$, with the distinct horizontal

thermal layer in the core, the temperature distribution will be stratified in the mid-core while the fluid motion therein would remain almost stagnant. Unfortunately no experiments have, as yet, been available for Pr < 1 to verify the above prediction.

[2] $\dfrac{1}{A(PrRa_H)^{\frac{1}{4}}} \gtrsim 1, \quad A^2 << 1$

Under this condition, from Eq. (3.144), conduction becomes important in the core and from Eq. (3.146), the horizontal thermal layer, δ_y, becomes of order

$$\frac{\delta_y}{H} \sim \frac{1}{A(PrRa_H)^{\frac{1}{4}}} \gtrsim 1 \tag{3.155}$$

Thus, there will no longer exist the distinct horizontal thermal layer in the core, instead some core fluid motion can be induced by the horizontal temperature gradients in the core in addition to the boundary layer driven circulating flows. Also the thermal boundary layer structure in the end region and thus the resulting flow driving mechanism will be modified according to the core temperature gradients. This flow regime also corresponds to the "intermediate flow regime" mentioned previously and will be considered later in the detailed analysis. The condition (3.147), i.e., $A(PrRa_H)^{\frac{1}{4}} > 1$, would thus be the necessary condition for the distinct boundary layer flow regime.

In this chapter, we have studied the global flow characteristics according to three different balances: the balance between

buoyancy and viscous forces in the core in Case I, the balance between buoyancy and inertia forces in the core in Case II and the balance between convection and conduction in the end with the additional force balance according to Pr. In what follows, considerations will be given both to the core flow structure of the intermediate flow regime and to the possible flow subregimes in the boundary layer flow regime of Case III.

CHAPTER IV

DETAILED VIEW OF THE FLOW CHARACTERISTICS

In the previous analysis, the core flow characteristics were studied globally according to three different cases. In Case I, the balance was made between buoyancy and viscous forces in the core and the core flow pattern was shown to be parallel whereas the core flow pattern was shown to be non-parallel in Case II, in which the balance was made between buoyancy and inertia forces in the core.

In Case III, the balance was made between convection and conduction in the end region. In addition, a balance was made in the end region between buoyancy and viscous forces for $Pr \gtrsim 1$ (including $Pr >> 1$) and between buoyancy and inertia forces for $Pr \lesssim 1$. In Case III, when there exist distinct horizontal thermal layers in the core the flow was shown to be driven by the boundary layers in the end region (called boundary-layer flow regime). In this situation the core flow structure was shown to be parallel for $Pr >> 1$, while the fluid motion is expected to remain almost stagnant in the mid-core both for $Pr \sim 1$ and $Pr < 1$. In addition, when the flow is driven by the end, there may appear some flow subregimes in the core due to the local interactions of the end and horizontal boundary layers. The occurrence of such flow subregimes will change the global core flow patterns, and their characteristic length scales would also be different from the geometric length scales. It thus becomes important to be able to predict the conditions under which flow subregimes are present and to estimate their length scales to

determine the core flow pattern.

In the analysis of Case III, in addition to the boundary layer flow regime the term "Intermediate Flow Regime" was defined in the sense that its flow and heat transfer characteristics would lie between the flow regime wherein the flow is driven in the core [Cases I and II] and that the driver is in the end region [boundary layer flow regime in Case III]. For such a flow regime, since it was not clear whether the geometric length scales are appropriate for the description of core flow structure, no global analysis of the flow pattern was made.

In what follows, consideration will be given to the prediction of the possible flow subregimes in the boundary layer flow regime and also to the prediction of the core flow pattern in the intermediate flow regime, both of which could not be predicted from the global analysis.

4.1 Prediction of Flow Subregimes in the Boundary Layer Flow Regime

4.1.1 Working Equations

The characteristic length scales of either the core flow structure in the intermediate flow regime or the expected flow subregimes in the boundary layer flow regime may be different from the geometric length scales. We thus replace the geometric length scales h_c and ℓ_c in the dimensionless equations (2.13) and (2.15),

which are to be specified in the course of analysis. In addition, as it is seen from the global analysis that the basic equations show singular behaviour at the horizontal boundaries, in order to account for that we introduce other multiple scales for the vertical coordinate y as

$$y = y, \qquad \hat{y} = \frac{y}{\varepsilon_h} \tag{4.1}$$

where

$$\varepsilon_h \sim \frac{\delta_h}{h_c} \tag{4.2}$$

and δ_h is an arbitrary horizontal layer to be properly specified in the analysis. The characteristic stream function is also to be specified according to δ_h concerned.

Introducing the derivatives of multiple scales (4.1) into Eqs. (2.13) and (2.15) and replacing H and L by h_c and ℓ_c, we then have

$$\frac{1}{\varepsilon_x}\frac{1}{\varepsilon_h}\frac{\partial(\xi,\psi)}{\partial(\eta,\hat{y})} + \frac{1}{\varepsilon_x}\frac{\partial(\xi,\psi)}{\partial(\eta,y)} + \frac{1}{\varepsilon_h}\frac{\partial(\xi,\psi)}{\partial(\zeta,\hat{y})} + \frac{\partial(\xi,\psi)}{\partial(\zeta,y)} = \frac{\beta g \Delta T \delta_x^* h_c}{\nu_R^2}\left(\frac{1}{\varepsilon_x}\frac{\partial\theta}{\partial\eta} + \frac{\partial\theta}{\partial\zeta}\right) + \frac{\nu \ell_c}{\nu_R h_c}\left(\frac{A_c^2}{\varepsilon_x^2}\frac{\partial^2\xi}{\partial\eta^2} + 2\frac{A_c^2}{\varepsilon_x}\frac{\partial^2\xi}{\partial\eta\partial\zeta} + A_c^2\frac{\partial^2\xi}{\partial\zeta^2} + \frac{1}{\varepsilon_h^2}\frac{\partial^2\xi}{\partial\hat{y}^2} + \frac{2}{\varepsilon_h}\frac{\partial^2\xi}{\partial\hat{y}\partial y} + \frac{\partial^2\xi}{\partial y^2}\right) \tag{4.3}$$

$$\frac{1}{\varepsilon_x}\frac{1}{\varepsilon_h}\frac{\partial(\theta,\psi)}{\partial(\eta,\hat{y})} + \frac{1}{\varepsilon_x}\frac{\partial(\theta,\psi)}{\partial(\eta,y)} + \frac{1}{\varepsilon_h}\frac{\partial(\theta,\psi)}{\partial(\zeta,\hat{y})} + \frac{\partial(\theta,\psi)}{\partial(\zeta,y)} = \frac{\alpha \ell_c}{\nu_R h_c}\left(\frac{A_c^2}{\varepsilon_x^2}\frac{\partial^2\theta}{\partial\eta^2} + 2\frac{A_c^2}{\varepsilon_x}\frac{\partial^2\theta}{\partial\eta\partial\zeta} + A_c^2\frac{\partial^2\theta}{\partial\zeta^2} + \frac{1}{\varepsilon_h^2}\frac{\partial^2\theta}{\partial\hat{y}^2} + \frac{2}{\varepsilon_h}\frac{\partial^2\theta}{\partial\hat{y}\partial y} + \frac{\partial^2\theta}{\partial y^2}\right) \tag{4.4}$$

where $A_c = \frac{h_c}{\ell_c}$ and δ_x replaces ℓ in Eq. (4.3)

4.1.2 Flow Subregimes near the End Region

It was mentioned earlier that flow subregimes are expected in the boundary-layer flow regime due to the interaction of the end and horizontal boundary layers. We first consider the situation in which the end region boundary-layer flow turns around the upper corner of the hot wall (or lower corner of the cold wall). In this situation, since the velocity has different values near the two rigid boundaries at the corner, the gradients of velocity become very large so that the viscous friction is supposed to be very large at the horizontal boundaries near the corner. In this sense, the present situation is physically similar to the case of two-dimensional flow in a corner due to one rigid plane sliding on another with constant inclination angle $\frac{\pi}{2}$, although the flow herein is driven by the buoyancy force within the thermal boundary layer at the end walls.

When the heated boundary-layer flow turns around the corner, the streamlines of the heated flow can be deflected due to the large viscous friction there. If the streamline deflection is large, some of the unheated flow entrained by the viscous shear of heated boundary-layer flow can be blocked so that it does not reach

the opposite end. In this way, closed streamlines could appear as flow subregimes such as secondary cells. However, this does not mean that the heated boundary-layer flow is also closed. Even though the heated flow is deflected near the corner, it will soon rise up and will circulate along the horizontal boundaries developing the horizontal thermal layers in the core. Otherwise, there will not exist distinct horizontal thermal layers in the core, so that the thermal boundary layer structure at the end walls will be altered and the distinct boundary-layer flow regmie will not exist. As a matter of fact, secondary cells near the end region were observed in some experiments and our attention here is focused on the prediction of such secondary cells considering the proper force balances. The inferred flow pattern for the above situation, which is actually based on the experimental observations, is approximately as indicated in Fig. 2.

If we consider the globally clear driving mechanism of the present situation, it can be inferred that the extent of the streamline deflection will largely depend on the interaction of the inertia of the buoyancy driven boundary-layer flow and the viscous friction within an arbitrary horizontal layer δ_h along the horizontal boundaries. Since the heated boundary layer flow will circulate across the top of the enclosure through the horizontal thermal layer δ_y, specifying δ_y as δ_h in (4.2), from Eq. (4.3), the proper force balance of the boundary layer inertia and horizontal viscous friction for that interaction can be represented as

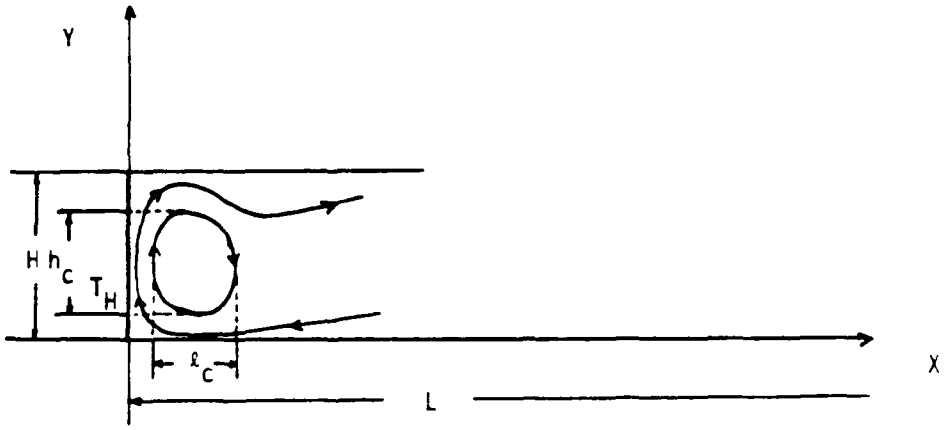

Figure 2. Approximate Representation of the Flow Pattern of Concern near the End Region

$$\frac{1}{\varepsilon_x} \sim \frac{\nu \ell_c}{\Psi_R h_c} \frac{1}{\varepsilon_h^2} \tag{4.5}$$

and this gives

$$\ell_c \sim \frac{\varepsilon_h^2}{\varepsilon_x} \frac{\Psi_R h_c}{\nu} \tag{4.6}$$

Since the characteristic values of Ψ_R and ε_x in (4.6) differ according to Prandtl numbers in the boundary-layer flow regime, we first consider the case of Pr $\gtrsim$ 1 (including Pr >> 1) and then that of Pr < 1 (as mentioned earlier, this always includes the case of Pr << 1).

(i) Pr $\gtrsim$ 1 (including Pr >> 1)

In this case, substituting the characteristic values $\Psi_R \sim \alpha Ra_H^{\frac{1}{4}}$ and $\varepsilon_x \sim \frac{A}{Ra_H^{\frac{1}{4}}}$ given in (3.89) and (3.90) into (4.6), the result is

$$\ell_c \sim \varepsilon_h^2 \frac{Ra_H^{\frac{1}{2}}}{PrA} h_c \tag{4.7}$$

To determine the length scales h_c and ℓ_c in (4.7) explicitly, one more relation is required. Considering the globally clear physical situation, however, no additional balance appropriate to the present situation seems to exist. But, based on the experimentally observed secondary cell patterns as shown in Fig. 2, it seems reasonable to suppose

$$h_c \sim H \tag{4.8}$$

From (4.7), we then obtain

$$\ell_c \sim \varepsilon_h^2 \frac{Ra_H^{\frac{1}{2}}}{Pr} L = \varepsilon_h^2 \sqrt{\frac{Gr_H}{Pr}} L \tag{4.9}$$

For large streamline deflection of the heated boundary layer flow near the corner, the horizontal thermal layer δ_y can be regarded as of order

$$\delta_y \sim O(H) \tag{4.10}$$

or
$$\varepsilon_h \sim \frac{\delta_y}{h_c} \sim \frac{\delta_y}{H} \sim 1 \tag{4.11}$$

From (4.9) and (4.11), we then have

$$\ell_c \sim \sqrt{\frac{Gr_H}{Pr}} L \tag{4.12}$$

In (4.12), when the arbitrary horizontal length scale ℓ_c is less than L, i.e., when $\frac{\ell_c}{L} < 1$, flow subregimes are expected to appear. This statement, though, is not the necessary and sufficient conditions for the occurrence of the flow subregimes, but it at least gives the necessary condition.

From (4.12), for $\frac{\ell_c}{L} < 1$

$$Pr^{\frac{1}{2}} > Gr_H^{\frac{1}{2}} \tag{4.13a}$$

or $$Pr > Ra_H^{\frac{1}{2}} \tag{4.13b}$$

For large values of Ra_H, the condition (4.13) can thus be satisfied for $Pr >> 1$.

The types of flow subregimes will depend on the length scale ℓ_c. From (4.8) and (4.12), it is seen that

$$\frac{h_c}{\ell_c} \sim \sqrt{\frac{Pr}{Gr_H}}\ A \tag{4.14}$$

When

$$APr^{\frac{1}{2}} \sim Gr_H^{\frac{1}{2}} \tag{4.15a}$$

or $$APr \sim Ra_H^{\frac{1}{2}} \tag{4.15b}$$

we find

$$\frac{h_c}{\ell_c} \sim 1 \tag{4.16}$$

This indicates that the flow subregime will appear as secondary cells near the end region. Considering the global flow characteristics in the core for $Pr >> 1$, however, patterns of multi-cells are not expected to the present situation.

(ii) <u>$Pr < 1$</u>

If we substitute the characteristic values of $\Psi_R \sim A(PrRa_H)^{\frac{1}{4}}$

and $\varepsilon_x \sim \frac{A}{(PrRa_H)^{\frac{1}{4}}}$ given in (3.130) and (3.131) into (4.6) and also supposing $h_c \sim H$, we obtain

$$\ell_c \sim \varepsilon_h^2 \, Gr_H^{\frac{1}{2}} \, L \tag{4.17}$$

For large streamline deflection, from (4.10) and (4.11) we may also put $\varepsilon_h \sim 1$. From (4.17), we then have

$$\ell_c \sim Gr_H^{\frac{1}{2}} \, L \tag{4.18}$$

Since $Gr_H >> 1$ for $Pr < 1$ in the boundary layer flow regime, from (4.18) we find

$$\frac{\ell_c}{L} \sim Gr_H^{\frac{1}{2}} > 1 \tag{4.19}$$

This indicates that no flow subregimes are expected near the end region for $Pr < 1$.

From the above analysis, flow subregimes near the end region are expected only for $Pr >> 1$. This is due to the fact that in the case of $Pr \sim 1$ and $Pr < 1$, the inertia of the boundary layer flow is strong enough to overcome the viscous friction near the corner while it turns around there, so that no appreciable streamline deflection occurs near the end region.

Experimentally secondary cells near the end region were observed in the work of Ostrach et. al. [31] for $A = 0.2$, $(Ra_H A)^2 \sim 10^{13}$ and $Pr = 1.38 \times 10^3$ and Kamotani et. al [33] for $A = 0.2$, $Ra_H = 4.8 \times 10^4$ and $Pr = 965$. In [31], secondary cells appeared

for somewhat higher values of Ra_H than the predicted value. But in that case, the horizontal boundaries are semi-conducting rather than adiabatic. The results in [33] show very good agreement with the above prediction. In the experiment of Simpkins and Dudderar [38], secondary cells were also observed and the critical Rayleigh number for the occurrence of secondary cells is given by

$$(Ra_H)_c \, A^{3/4} \sim 6.4 \times 10^5 \pm 10\% \qquad (4.20)$$

which has an aspect ratio dependence for the range of $0.1 \lesssim A \lesssim 4$. The condition (4.20) does not show good agreement with the results of [31] and [33]. In the experiments of [31], [33] and [38], when secondary cells appeared, there was only one in each end of the cavity and the core flow was not parallel. No experiments have been conducted, as yet, for $A \lesssim 0.1$ with adiabatic horizontal boundaries under the condition indicated in (4.15) for the existance of secondary cells. Since for $Pr \gg 1$, the global analysis for the parallel core flow structure in the boundary layer flow regime yields only the condition $A^2 \ll 1$, it would be interesting to make observation under the condition (4.15).

In the numerical work of Jhaveri and Rosenberger [40], for $A = 0.1$, $Sc = 0.5$, $Pr = 0.7$ and $Gr_H = 3.3 \times 10^4$, the resulting flow profile shows the onset of a recirculation cell at each interface. It should be noted that this cell is due to the coupling of mass flux at the interface with the transport quantities.

4.1.3 Flow Subregimes in the Core

In the preceding analysis, secondary cells were shown to be possible near the end region for $Pr \gg 1$. Here the possibility of flow subregimes is going to be examined away from the end region, i.e., in the core by considering the interaction of the inertia and viscous forces of the end driven core circulating flow along the long horizontal boundaries. This interaction was considered in the previous global analysis for $Pr \sim 1$. From that consideration, it was shown that the horizontal viscous layer is distinct in the core under the condition $ARa_H^{\frac{1}{4}} > Pr^{\frac{1}{2}}$ and the corresponding flow pattern remains nearly stagnant in the mid-core. Since the condition required is $ARa_H^{\frac{1}{4}} > 1$ for the existence of a distinct horizontal thermal layer in the core, the question naturally arises what the core flow pattern would be like under the condition $1 < ARa_H^{\frac{1}{4}} < Pr^{\frac{1}{2}}$, wherein the horizontal thermal layer is distinct but the horizontal viscous layer is of order, $\delta_v > H$. The present analysis is thus concerned in predicting the core flow pattern in that situation.

In the analysis the possibility is implicitly disregarded for $Pr \gg 1$, because in that case, the inertia is negligible and globally the core flow structure was shown to be parallel unless there appear secondary cells near the end region.

If the balance is made for the interaction between the inertia and viscous vorces within the arbitrary horizontal layer δ_h, from

Eq. (4.3) it can be represented as

$$\frac{1}{\epsilon_h} \sim \frac{\nu \ell_c}{\Psi_R h_c} \frac{1}{\epsilon_h^2} \tag{4.21}$$

Since we are considering the momentum balance of the circulating flow, the arbitrary horizontal layer δ_h can be regarded as the horizontal viscous layer δ_v. The characteristic stream function Ψ_R in (4.21) thus needs to be replaced by the modified stream function $\bar{\Psi}_R$ for δ_v. We first consider the case of $Pr \sim 1$ and then that of $Pr < 1$.

(i) $\underline{Pr \sim 1}$

Replacing Ψ_R by $\bar{\Psi}_R$ in (4.21) and substituting the characteristic value of $\bar{\Psi}_R$ from Appendix D, we find

$$\ell_c \sim \epsilon_h \frac{Ra_H^{\frac{1}{4}}}{Pr^{\frac{1}{2}}} h_c \tag{4.22}$$

Here we also need one more relation to determine the length scales h_c and ℓ_c explicitly. However, there does not seem to exist an appropriate balance for the present situation. As was done previously, if we suppose $h_c \sim H$, for large streamline deflection, as in (4.11) we may put

$$\epsilon_h \sim \frac{\delta_v}{H} \sim 1 \tag{4.23}$$

From (4.22) and (4.23), we then obtain

$$\ell_c \sim \frac{Ra_H^{\frac{1}{4}}}{Pr^{\frac{1}{2}}} H \tag{4.24}$$

For $\frac{\ell_c}{L} < 1$, from (4.24)

$$\frac{Ra_H^{\frac{1}{4}}}{Pr^{\frac{1}{2}}} A < 1 \tag{4.25a}$$

or $$ARa_H^{\frac{1}{4}} < Pr^{\frac{1}{2}} \tag{4.25b}$$

Since $ARa_H^{\frac{1}{4}} > 1$ for the boundary flow regime, from (4.25) flow subregimes are expected in the core under the condition

$$\frac{1}{Ra_H^{\frac{1}{4}}} < A < \frac{Pr^{\frac{1}{2}}}{Ra_H^{\frac{1}{4}}} \tag{4.26}$$

when $Pr \gtrsim 1$, from (3.123) $\delta_y \gtrsim \delta_v$, and thus for $\delta_v \sim H$ in (4.23), δ_y is also of order O(H). In this situation, no distinct horizontal thermal layer exists in the core and the flow regime corresponds to the intermediate flow regime. Therefore in the boundary layer flow regime, from (4.26), as long as $ARa_H^{\frac{1}{4}} > 1$, no flow subregimes are expected in the core for $Pr \gtrsim 1$, but they are expected for Pr slightly greater than 1 (for example, water).

The types of flow subregimes, as mentioned earlier, will depend on the length scale ℓ_c. From (4.25), we find

$$\frac{L}{\ell_c} \sim \frac{Pr^{\frac{1}{2}}}{ARa_H^{\frac{1}{4}}} \gtrsim n \tag{4.27}$$

and

$$\frac{h_c}{\ell_c} \sim \frac{Pr^{\frac{1}{2}}}{Ra_H^{\frac{1}{4}}} \tag{4.28}$$

where n denotes an arbitrary integer approximating the ratio of $\frac{L}{\ell_c}$.

From (4.27), the value of n will indicate the patterns of flow subregimes in the core. For example, when n = 3 this may imply the appearance of three cells in the core. However, since $ARa_H^{\frac{1}{4}} > 1$ and the case of $Pr >> 1$ is neglected here, the ratio of $\frac{L}{\ell_c}$ in (4.27) cannot be a much larger value than 1. Further, from (4.28), for large values of Ra_H we find

$$\frac{h_c}{\ell_c} \sim \frac{H}{\ell_c} < 1 \tag{4.29}$$

for $Pr \sim 1$. Therefore, patterns of multi-cells are not expected to appear in this situation.

(ii) <u>Pr < 1</u>

In this case, from (3.151) it is seen that the horizontal thermal layer extends beyond the horizontal viscous layer, i.e., $\delta_y > \delta_v$. Thus for $\delta_v \sim H$ in (4.23), δ_y is of order, $\delta_y > H$. Then there does not exist a distinct horizontal thermal layer in the core and the flow regime in this situation corresponds to the intermediate flow regime. For Pr < 1, no flow subregime are, therefore, expected in the core as well as near the end region in the boundary layer flow regime.

Experimentally a single slow central circulating flow subregime in the core was observed in the work of Imberger [29] for Pr = 7, $Ra_H = 1.11 \times 10^8$ and A = 0.02. This shows good agreement with the above prediction. No experiments with the fluids of Pr < 1 have been conducted in the boundary layer flow regime, as yet, for the present configuration.

Summarizing the above analysis, in the boundary layer flow regime, flow subregimes such as secondary cells are possible near the end region for Pr >> 1 whereas they are possible in the core for Pr ~ 1 (except Pr $\gtrsim$ 1). No flow subregimes, however, are expected for fluids with Pr < 1.

4.2 Prediction of Core Flow Pattern in the Intermediate Flow Regime

4.2.1 Working Equations

In the intermediate flow regime, there does not exist distinct horizontal thermal layer in the core. Thus, there would be no singular behaviour of the basic equations with respect to the horizontal boundaries so that it is not needed to introduce the other multiple scales with respect to y as in (4.1). In this situation the working equations (4.3) and (4.4) simply reduces to

$$\frac{1}{\ell_x}\frac{\partial(\xi,\psi)}{\partial(\eta,\zeta)} + \frac{\partial(\xi,\psi)}{\partial(\zeta,\zeta)} = \frac{\beta g \Delta T \delta_x^* h_c}{\nu_x^2}\left(\frac{1}{\ell_x}\frac{\partial\theta}{\partial\eta} + \frac{\partial\theta}{\partial\zeta}\right) + \frac{\nu \ell_c}{\nu_x h_c}\left(\frac{A_c^2}{\ell_x^2}\frac{\partial^2\xi}{\partial\eta^2}\right.$$

$$\left. + 2\frac{A_c^2}{\ell_x}\frac{\partial^2\xi}{\partial\eta\partial\zeta} + A_c^2\frac{\partial^2\xi}{\partial\zeta^2} + \frac{\partial^2\xi}{\partial\zeta^2}\right) \qquad (4.30)$$

$$\frac{1}{\varepsilon_n}\frac{\partial(\theta,\psi)}{\partial(\eta,\gamma)} + \frac{\partial(\theta,\psi)}{\partial(\zeta,\gamma)} = \frac{\alpha \ell_c}{\nu_n h_c}\left(\frac{A_r^2}{\varepsilon_n^2}\frac{\partial^2\theta}{\partial\eta^2} + 2\frac{A_r^2}{\varepsilon_n}\frac{\partial^2\theta}{\partial\eta\partial\zeta} + A_r^2\frac{\partial^2\theta}{\partial\zeta^2} + \frac{\partial^2\theta}{\partial\gamma^2}\right) \quad (4.31)$$

4.2.2 Prediction of Core Flow Pattern

The balances in Eqs. (4.30) and (4.31) which will properly describe the fluid physics in the intermediate flow regime are not readily apparent. However, as mentioned previously, it is supposed that the flow and heat transfer characteristics in the intermediate flow regime would lie between the flow regime wherein the flow is driven in the core and that wherein the flow is driven by the boundary layer in the end region. In other words, it may be said that the balances made in both flow regimes can now be made in the intermediate flow regime. It is thus from this arguement that the balances are going to be made in the following analysis.

In the flow regime wherein the flow is driven in the core, the force balances are made in the core either between the buoyancy and viscous forces or between the buoyancy and inertia forces according to Pr. In the end driven flow regime, the balances are made in the end region either between the buoyancy and viscous forces or between the buoyancy and inertia forces. In addition, in the former case the heat convection and conduction

terms become of equal order in the core for higher value of Ra_H (i.e., for $Ra_H A^2 \sim 1$ in Case I) whereas both terms are balanced in the end region in the latter case. Therefore, basically two balances can be made herein in both the end and core regions either from the force balances or from the heat balances. In the following, we first make the heat balances in both end and core regions. Based on the heat balances, the force balances will then be made appropriately and we will see what the results imply. Other force balances will also be considered if necessary.

From Eq. (4.31), the balance between convection and conduction in the end region can be represented as

$$\frac{1}{\varepsilon_x} \sim \frac{\alpha \ell_c}{\tau_R h_c} \frac{A_c^2}{\varepsilon_x^2} \tag{4.32}$$

and in the core

$$1 \sim \frac{\alpha \ell_c}{\Psi_R h_c} \tag{4.33}$$

Since

$$\varepsilon_x \sim \frac{\delta_x}{\ell_c} \tag{4.34}$$

from (4.32) and (4.33), we obtain

$$\Psi_R \sim \frac{\alpha}{A_c} \tag{4.35}$$

and

$$\delta_x \sim \frac{h_c^2}{\ell_c} \tag{4.36}$$

The explicit forms of the characteristic quantities in (4.35) and (4.36) can be determined from the length scales of h_c and ℓ_c obtained by proper force balances for the motions induced by both the core and end temperature gradients. From the global analysis, it is evident that the Pr acts as a parameter. Thus this will be done according to the Pr.

(i) Pr ~ 1

In this case, the balance between the buoyancy and viscous forces are appropriate. We first consider the balance in the end region. From Eq. (4.30), this balance can be represented as

$$\frac{\beta g \Delta T \delta_x^2 h_c}{\Psi_R^2} \frac{1}{\ell_x} \sim \frac{\nu \ell_c}{\Psi_R h_c} \frac{A_c^2}{\ell_x^2} \tag{4.37}$$

From (4.35),(4.36) and (4.37), we find

$$\ell_c^* \sim \frac{\beta g \Delta T h_c^3}{\alpha \nu} h_c^* \tag{4.38a}$$

or

$$\left(\frac{h_c}{\ell_c}\right)^* \sim \frac{\alpha \nu}{\beta g \Delta T h_c^3} \tag{4.38b}$$

In order to determine the length scales h_c and ℓ_c explicitly, one more force balance is required. Firstly, if we take the balance between the buoyancy and viscous forces in the core, from Eq. (4.30)

AD-A124 995 PREDICTION OF NATURAL CONVECTION FLOW PATTERN IN LOW-ASPECT RATIO ENCLOSU..(U) CASE INST OF TECH CLEVELAND OHIO FLUID THERMAL AND AEROSPACE S..

2/2

UNCLASSIFIED J LEE ET AL. 26 MAY 82 FTAS/TR-82-158 F/G 12/1 NL

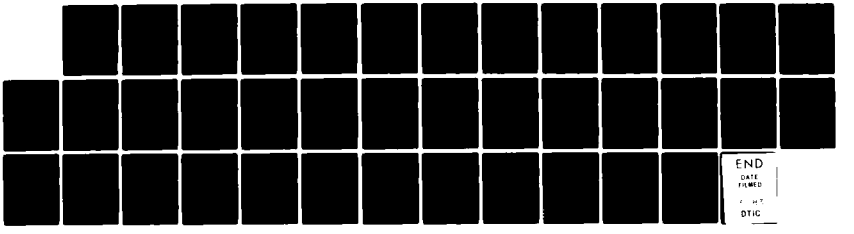

END

DATE FILMED

DTIC

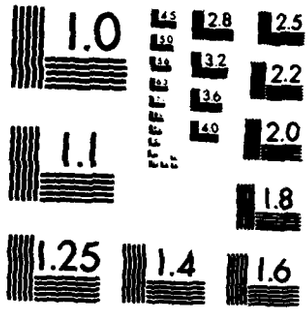

MICROCOPY RESOLUTION TEST CHART
NATIONAL BUREAU OF STANDARDS-1963-A

this can be represented as

$$\frac{\beta g \Delta T \delta_x^2 h_c}{\nu_e^2} \sim \frac{\nu \ell_c}{\nu_e h_c} \tag{4.39}$$

From (4.35), (4.36) and (4.39), we then have

$$\left(\frac{h_c}{\ell_c}\right)^4 \sim \frac{\alpha \nu}{\beta g \Delta T h_c^3} \tag{4.40}$$

which is identical to the relation (4.38). Thus this force balance does not give any more information.

Secondly, if we consider the possible interaction of the viscous forces between the end and core region, one additional force balance can be inferred, that is, the balance between the viscous force in the end and the viscous force in the core. From Eq. (4.30) this balance can be represented as

$$\frac{A_c^2}{\epsilon_x^2} \sim A_c^2 \tag{4.41}$$

This gives

$$\epsilon_x \sim 1 \tag{4.42}$$

or

$$\delta_x \sim \ell_c \tag{4.43}$$

From (4.36) and (4.43), we find

$$A_c^2 \sim 1 \tag{4.44}$$

so that $\ell_c \sim h_c$ (4.45)

From (4.38) and (4.45), we then obtain

$$h_c^3 \sim \frac{\alpha\nu}{\beta g \Delta t} \tag{4.46}$$

and this shows

$$\frac{h_c}{H} \sim \frac{1}{Ra_H^{1/3}} \tag{4.47}$$

Since $A^2 Ra_H >> 1$ for the intermediate flow regime, for $A^2 << 1$, Ra_H is a large value. From (4.47), we thus find

$$\frac{h_c}{H} < 1 \tag{4.48}$$

The relations (4.45) and (4.48) indicate the existence of very small cells in the core. No observation of such cells has, as yet, been reported within the parametric ranges of concern here (i.e., $A^2 Ra_H >> 1$, $ARa_H^{\frac{1}{4}} \lesssim 1$), although the data are not extensive. Physically, the appearance of very small cells in the core, in general, does not seem to be a plausible situation, and thus the balance between the viscous forces in the end and core region seems to be inappropriate for the present situation.

If, as previously, we suppose

$$h_c \sim H \tag{4.49}$$

from (4.38), we obtain

$$\ell_c \sim Ra_H^{\frac{1}{4}} H \tag{4.50}$$

From (4.49) and (4.50), Ψ_R and δ_x in (4.35) and (4.36) can then be represented as

$$\Psi_R \sim \alpha Ra_H^{\frac{1}{4}} \tag{4.51}$$

and $$\delta_x \sim \frac{H}{Ra_H^{\frac{1}{4}}} \tag{4.52}$$

From (4.51) and (4.52), it is seen that the expression for Ψ_R and δ_x herein are similar to those of the boundary-layer flow regime. This may imply that the flow characteristics in the intermediate flow regime concerned here are rather closer to those in the boundary-layer flow regime. However, since $ARa_H^{\frac{1}{4}} \lesssim 1$ in the intermediate flow regime, from (4.50) we find

$$\frac{\ell_c}{L} \sim ARa_H^{\frac{1}{4}} \lesssim 1 \tag{4.53}$$

and for $ARa_H^{\frac{1}{4}} < 1$

$$\frac{\ell_c}{L} < 1, \tag{4.54}$$

which indicates the existence of flow subregimes in the core due to the core temperature gradients. The length scale ℓ_c, which is a certain fraction of L in (4.54), may thus indicate what type of flow subregimes will appear.

When $ARa_H^{\frac{1}{4}} < 1$, from (4.50) we may write

$$\frac{L}{\ell} \sim \frac{1}{ARa_H^{\frac{1}{4}}} \approx n \tag{4.55}$$

where n is an arbitrary integer approximating the ratio of $\frac{L}{\ell_c}$.

For large values of Ra_H such that $Ra_H A^2 \gg 1$ for $A^2 \ll 1$, from (4.50) we also find

$$\frac{h_c}{\ell_c} \sim \frac{1}{Ra_H^{\frac{1}{4}}} < 1 \tag{4.56}$$

From (4.55) and (4.56), since

$$\frac{h_c}{\ell_c} \sim \frac{L}{\ell_c} A \approx An \tag{4.57}$$

we then find

$$1 < n < \frac{1}{A} \tag{4.58}$$

This indicates that patterns of multi-cells are possible in the core for small values of A, i.e., for $A^2 \ll 1$.

When $ARa_H^{\frac{1}{4}} \sim 1$, from (4.50) $\frac{\ell_c}{L} \sim 1$. In this situation, no apparent flow subregimes are expected and it is not readily clear what type of flow patterns will appear in the core.

When $ARa_H^{\frac{1}{4}} > 1$, $\frac{\ell_c}{L} > 1$ and thus, no flow subregimes are expected This is the case of boundary-layer flow regime. It is evident from the global analysis that no flow subregimes are expected by the core temperature gradient in the boundary-layer flow regime.

Few experimental data available for the present situation are found in the Imberger's experiment [29]. In [29], when $ARa_H^{\frac{1}{4}} \sim 1$, e.g., Pr = 7.0, $Ra_H = 8.04 \times 10^6$ and A = 0.02, some part of the core flow turns around before it reaches the end region. For $ARa_H^{\frac{1}{4}} < 1$, however, the flow structure is parallel in the core and no flow subregimes are observed. Nevertheless, based on the supposition of $h_c \sim H$, rather plausible core configurations seem to have been drawn, and more experiments are needed to verify the possible appearance of flow subregimes in the intermediate flow regime of concern here.

(ii) Pr >> 1

For Pr >> 1, globally the core flow structure was shown to be parallel in both Case I and Case III. In this case, due to the high viscous shear, it is not likely that the development occurs in such a way that first the parallel core flow structure in Case I becomes the non-parallel core flow structure in the intermediate flow regime and then the non-parallel core flow structure reverts to the parallel core flow structure in Case III. Thus the parallel core flow structure is still expected in the intermediate flow regime for Pr >> 1. Actually in the experiment done so far for Pr >> 1 for the present configuration, e.g., Kamotani et. al. [33] and Simpkins and Dudderar [38], the parallel core flow pattern was observed for the most ranges of the parameter Ra_H unless, as mentioned earlier, secondary cells appear near the end in the boundary-layer flow regime.

(iii) Pr < 1

In this case, the appropriate force balance is that between the buoyancy and inertia forces. We first consider the force balance in the end region. From (4.30), this balance can be represented as

$$\frac{1}{\varepsilon_x} \sim \frac{\beta g \Delta T \delta_x^2 h_c}{\nu_x^2} \frac{1}{\varepsilon_x} \tag{4.59}$$

From (4.35), (4.36) and (4.59), we then obtain

$$\left(\frac{h_c}{\ell_c}\right)^4 \sim \frac{\alpha^2}{\beta g \Delta T h_c^3} \tag{4.60}$$

In order to determine the length scales h_c and ℓ_c explicitly, one more force balance is required. Since the balance between the buoyancy and inertia forces in the core yields the same relation as in (4.59), it does not give any more information. Assuming the possible interaction of the inertia forces between the end and core region, one additional force balance, that is, the balance between the inertia in the end and the inertia in the core, could be inferred. From Eq. (3.40), this balance can be represented as

$$\frac{1}{\varepsilon_x} \sim 1 \tag{4.61}$$

and this gives

$$\varepsilon_x \sim 1 \tag{4.62}$$

or from (4.34)

$$\delta_x \sim \ell_c \tag{4.63}$$

From (4.36) and (4.63), we find

$$A_c^2 \sim 1 \tag{4.64}$$

so $$\ell_c \sim h_c \tag{4.65}$$

From (4.60) and (4.65), we then have

$$h_c^3 \sim \frac{\alpha^2}{\beta g \Delta T} \tag{4.66}$$

and this gives

$$\frac{h_c}{H} \sim \frac{1}{(PrRa_H)^{1/3}} \tag{4.67}$$

For large values of Ra_H such that $Ra_H A^2 \gg 1$ for $A^2 \ll 1$, it is supposed

$$\frac{h_c}{H} < 1 \tag{4.68}$$

except for extremely small Pr. The relations (4.65) and (4.68) also indicate the existence of very small cells in the core. For $Pr < 1$, no experiment has, as yet, been conducted for the present configuration within the parametric ranges corresponding to the intermediate flow regime of concern here (i.e., $A^2 Ra_H \gg 1$, $A(PrRa_H)^{\frac{1}{4}} \lesssim 1$).

In (4.67), when Pr is extremely small, it is possible that

$$\frac{h_c}{H} \sim \frac{1}{(PrRa_H)^{1/3}} \sim 1 \tag{4.69}$$

In this case, patterns of multi-cells may be possible in the core. However, in order that $PrRa_H \sim 1$, Pr should be of order $O(10^{-4})$ or less than that for the common ranges of the parameters, $A \lesssim 0.1$ and $Ra_H \gtrsim 10^4$ such that $Ra_H A^2 >> 1$. Thus, in general, that does not seem to be a realistic situation.

If we suppose $h_c \sim H$, from (4.60) we obtain

$$\ell_c \sim (PrRa_H)^{\frac{1}{4}} H \tag{4.70}$$

The characteristic quantities Ψ_R and δ_x in (4.35) and (4.36) can then be represented as

$$\Psi_R \sim \alpha(PrRa_H)^{\frac{1}{4}} \tag{4.71}$$

and

$$\delta_x \sim \frac{H}{(PrRa_H)^{\frac{1}{4}}} \tag{4.72}$$

These characteristic quantities are similar to those of the boundary-layer flow regime for Pr < 1. This also implies that the flow characteristics in this intermediate flow regime are closer to those in the boundary layer flow regime.

Since $A(PrRa_H)^{\frac{1}{4}} \lesssim 1$ in the intermediate flow regmie for Pr < 1, from (4.70) we find

$$\frac{\ell_c}{L} \sim A(PrRa_H)^{\frac{1}{4}} \lesssim 1 \tag{4.73}$$

and for $A(PrRa_H)^{\frac{1}{4}} < 1$

$$\frac{\ell_c}{L} < 1 \tag{4.74}$$

This also implies the existence of flow subregimes in the core and the length scale of ℓ_c will indicate the types of such flow subregimes.

When $A(PrRa_H)^{\frac{1}{4}} < 1$, from (4.70) we may write

$$\frac{L}{\ell_c} \sim \frac{1}{A(PrRa_H)^{\frac{1}{4}}} \approx n \tag{4.75}$$

where n denotes an arbitrary integer approximating the ratio of $\frac{L}{\ell_c}$. Except for extremely small values of Pr, from (4.70) we also find

$$\frac{h_c}{\ell_c} \sim \frac{1}{(PrRa_H)^{\frac{1}{4}}} < 1 \tag{4.76}$$

From (4.75) and (4.76), since

$$\frac{h_c}{\ell_c} \sim A\frac{L}{\ell_c} \approx An \tag{4.77}$$

we thus find

$$1 < n < \frac{1}{A}, \tag{4.78}$$

which indicates that patterns of multi-cells are possible in the core for $A^2 << 1$.

When $A(PrRa_H)^{\frac{1}{4}} \sim 1$, from (4.70), $\frac{\ell_c}{L} \sim 1$. In this situation, no apparent flow subregimes are expected and the core flow pattern is not readily clear.

When $A(PrRa_H)^{\frac{1}{4}} > 1$, $\frac{\ell_c}{L} > 1$ and thus no flow subregimes are expected. This is the case of boundary-layer flow regime. It is evident from the global analysis that no such flow subregimes are expected in the boundary-layer flow regime for $Pr < 1$.

In the above, although there do not exist any experimental data available for direct comparison, the core configuration drawn from the supposition of $h_c \sim H$ seems to be a rather more plausible situation than that obtained from the additional force balance between the inertia forces in the end and core region.

Utech et.al. [45] conducted an experiment with molten tin of $Pr \sim O(10^{-2})$. Their configuration is, although, similar to that considered here, it differs significantly in that the upper surface is free surface. Experiment shows a pattern of multi-cells in the core superimposing on the generally steady flow along the bottom and top of the boat. However, this is supposedly due to the vertical heat transfer through the open boat top.

In summary, in the intermediate flow regime, the core flow pattern is not parallel and flow subregimes such as secondary cells or patterns of multi-cells seem to be possible both for $Pr \sim 1$ and $Pr < 1$, whereas the parallel core flow pattern is still expected for $Pr >> 1$.

CHAPTER V

SUMMARY AND CONCLUDING REMARKS

Consideration has been given to the prediction of core flow pattern in a low aspect ratio rectangular enclosures. Globally core flow characteristics were studied according to the three different cases. With the information obtained from the global analysis, the core flow pattern was also examined in detail to predict the possible flow subregimes such as secondary cells.

In the analysis of Case I, the balance was made between buoyancy and viscous forces in the core. The analysis based on this force balance is valid within the parametric ranges of $Gr_H A^2 \lesssim 1$ and $Ra_H A^2 \lesssim 1$. In this flow regime, the core flow is parallel and the core temperature distribution is either purely linear or linear and stratified.

In Case II, the analysis is based on the balance between buoyancy and inertia forces in the core. The analysis in this case is limited to the parametric ranges of $Gr_H A^2 \gg 1$, $Pr^2 \ll \frac{1}{Gr_H A^2}$ such that $PrRa_H A^2 \ll 1$. The core flow is not parallel in this flow regime while the core temperature distribution is purely linear.

In both Cases I and II, the flow is driven in the core and no flow subregimes are expected. For $Ra_H A^2 \gg 1$, however, the driving force was shown to exist in the end region and this situation was considered as Case III.

In the analysis of Case III, the balance was made between convection and conduction in the end region. In addition, the balance was made in the end region between buoyancy and viscous forces for $Pr \gtrsim 1$ (including $Pr >> 1$) and between buoyancy and inertia forces for $Pr < 1$ (this always includes the case of $Pr << 1$).

In Case III, under the conditions, $ARa_H^{\frac{1}{4}} > 1$ for $Pr \gtrsim 1$ (including $Pr >> 1$) and $A(PrRa_H)^{\frac{1}{4}} > 1$ for $Pr < 1$, there exist distinct horizontal thermal layers adjacent to the horizontal boundaries in the core and the temperature distribution outside the horizontal thermal layers, i.e., in the mid-core, is stratified. The core flow is driven by the thermal boundary layers in the end region, and for $Pr >> 1$ the core flow pattern is parallel while the fluid motion remains nearly stagnant in the mid-core for $Pr \sim 1$ (i.e., Pr is about 1 or slightly greater than 1) and $Pr < 1$. In this flow regime (called the boundary-layer flow regime), flow subregimes such as secondary cells are expected to appear near the end region for $Pr >> 1$ under the condition $APr \sim Ra_H^{\frac{1}{4}}$, while in the core flow subregimes are expected for $Pr \sim 1$ (except $Pr \tilde{\sim} 1$) under the condition $\frac{1}{Ra_H^{\frac{1}{4}}} < A < \frac{Pr^{\frac{1}{4}}}{Ra_H^{\frac{1}{4}}}$.

When $ARa_H^{\frac{1}{4}} \lesssim 1$ for $Pr \gtrsim 1$ (including $Pr >> 1$) and when $A(PrRa_H)^{\frac{1}{4}} \lesssim 1$ for $Pr < 1$, the flow regime corresponds to the so called intermediate flow regime. In this flow regime, the core flow pattern is not parallel and flow subregimes such as secondary cells or patterns of multi-cells seem to be possible in the core for $Pr \sim 1$ and $Pr < 1$ whereas a parallel flow core pattern is still

expected for Pr >> 1. Summary of the results of the present analysis is given in Table 1.

By comparisons, predictions of core flow pattern made herein show good agreement with the existing experimental results for Pr $\sim$ 1 and Pr >> 1, although the data are not extensive. For Pr < 1, no experimental data for the present configuration are available, as yet, for direct comparison. More experiments are needed to verify the present predictions in order to understand the physics of the core flow pattern more clearly and to indicate the validity of the type of analysis presented herein. Clearly the analysis can be generalized for other configurations.

Based on the multiple scales technique, global prediction of the core flow pattern is generally satisfactory. Further work will be required to define the flow subregimes better. Nevertheless, it is thought that employing the ideas of multiple scales technique attempted herein can surely be applied to resolve many other complex problems.

TABLE 1. SUMMARY OF THE ANALYSIS

	BASIC BALANCES	SCALES	PHYSICAL CONDITIONS			CORE CONFIGURATIONS
CORE DRIVEN FLOW REGIME	Buoyancy ~ Viscous in the Core Horizontal Viscous ~ Vertical Viscous in the End	$v_R \sim \frac{\beta g \Delta T H^4}{\nu L}$ $\delta_x \sim H$	$Gr_H A^2 \ll 1$ $A^2 \ll 1$	$Ra_H A^2 \ll 1$		parallel flow pattern linear temperature distribution
				$Ra_H A^2 \sim 1$		parallel flow pattern linear & stratified temperature distribution
	Buoyancy ~ Inertia in the Core Inertia in the End ~ Inertia in the Core	$v_R \sim (\beta g \Delta T H^3)^{\frac{1}{2}}$ $\delta_x \sim L$	$Gr_H A^2 \gg 1$ $A^2 \ll 1$	$PrRa_H A^2 \gg 1$		non-parallel flow pattern linear temperature distribution
BOUNDARY LAYER FLOW REGIME	Convection ~ Conduction in the End Buoyancy ~ Viscous in the End	$v_R \sim Ra_H^{\frac{1}{4}}$ $\delta_x \sim \frac{H}{Ra_H^{\frac{1}{4}}}$	$Ra_H A^2 \gg 1$ $A^2 \ll 1$	$ARa_H^{\frac{1}{4}} \gg 1$	$Pr \sim 1$	distinct horizontal thermal layers exist stratified temperature distribution with stagnant fluid motion in the mid-core flow subregimes expected when $ARa_H^{\frac{1}{4}} < Pr^{\frac{1}{4}}$
					$Pr \gg 1$	distinct horizontal thermal layers exist parallel flow pattern stratified temperature distribution in the mid-core secondary cells expected near the end when $APr \sim Ra_H^{\frac{1}{4}}$
	Conv. ~ Cond. in the End Buoy. ~ Inertia in the End	$v_R \sim a(PrRa_H)^{\frac{1}{4}}$ $\delta_x \sim \frac{H}{(PrRa_H)^{\frac{1}{4}}}$		$A(PrRa_H)^{\frac{1}{4}} \gg 1$	$Pr \ll 1$*	distinct horizontal thermal layers exist stratified temperature distribution with stagnant fluid motion in the mid-core
INTERMEDIATE FLOW REGIME	Conv. ~ Cond. in both the End and Core Buoy. ~ Viscous in the End (or in the Core)	$v_R \sim Ra_H^{\frac{1}{4}}$ $\delta_x \sim \frac{H}{Ra_H^{\frac{1}{4}}}$	$Ra_H A^2 \gg 1$ $A^2 \gg 1$	$ARa_H^{\frac{1}{4}} \gg 1$	$Pr \gg 1$	non-parallel flow pattern patterns of multi-cells seem to be possible temperature varies in both x and y direction
					$Pr \sim 1$	parallel flow pattern temperature varies in both x and y direction
	Conv. ~ Cond. in both the End and Core Buoy. ~ Inertia in the End (or in the Core)	$v_R \sim a(PrRa_H)^{\frac{1}{4}}$ $\delta_x \sim \frac{H}{(PrRa_H)^{\frac{1}{4}}}$		$A(PrRa_H)^{\frac{1}{4}} \gg 1$	$Pr \gg 1$*	non-parallel flow pattern patterns of multi-cells seem to be possible temperature varies in both x and y direction

* This always includes the case of $Pr \sim 1$

REFERENCES

1. Ostrach, S., "Natural Convection in Enclosures", in Advances in Heat Transfer, vol. 8, Chapt. 3, Academic Press, (1972).

2. Catton, I., "Natural Convection in Enclosures", Proc. 6th Heat Transfer Conference, 1, pp. 13-31, (1978).

3. Ostrach S., "A Boundary Layer Problem in the Theory of Free Convection", Ph.D. Thesis, Brown University, Providence, R.I., (1950)

4. Batchelor, G.K., "Heat Transfer by Free Convection across a Closed Cavity between Vertical Boundaries at Different Temperatures", Quart. Appl. Math., 12, pp. 209-233 (1954).

5. Weinbaum, S., "Natural Convection in a Horizontal Circular Cylinder", J. Fluid Mech., 18, pp. 409-437, (1964).

6. Menold, E.R. and Ostrach, S., "Natural Convection in a Horizontal Cylinder at Large Prandtl Numbers", Case Inst. of Tech., Cleveland, Ohio, FTAS/TR-65-4 or AFOSR Tech. Rep. NO. AFOSR 65-2239 (1965).

7. Gill, A.E., "The Boundary-Layer Regime for Convection in a Rectangular Cavity", J. Fluid Mech., 26, Part 3, pp. 515-536, (1966).

8. Hantman, R. and Ostrach, S., "Natural Convection Inside a Horizontal Cylinder", Chem. Eng. Commun. vol. 9, pp. 213-243, (1981).

9. Ostrach, S. and Pnueli, D., "The Thermal Instability of Completely Confined Fluids Inside Some Particular Configurations", Trans. ASME, 85, Series C, (Nov. 1963).

10. Ostrach, S. and Menold, E.R., "Natural Convection in a Horizontal Cylinder", The Third All-Union Heat and Mass Transfer Conference, Minsk, B.S.S.R., U.S.S.R., (May, 1968).

11. Brooks, I. and Ostrach, S., "An Experimental Investigation of Natural Convection in a Horizontal Cylinder", J. Fluid Mech., 44, pp. 545-561, (1970).

12. Sabzevari, A. and Ostrach, S., "Experimental Studies of Natural Convection in a Horizontal Cylinder", Heat Transfer 1974, Fifth International Heat Transfer Conference, Vol. III, pp. 100-104, Tokyo, (Sept. 1974).

13. Martini, W.R. and Churchill, S.W., "Natural Convection Inside a Horizontal Cylinder", AICHE Jour., 6, pp. 251-257, (1960).

14. Eckert, E.R.G. and Carlson, W.O., "Natural Convection in an Air Layer Enclosed between Two Vertical Plates with Different Temperatures", Int. J. Heat Mass Transfer, 2, pp. 106-120, (1961).

15. Elder, J.W., "Laminar Free Convection in a Vertical Slot", J. Fluid Mech. 24, pp. 823-843, (1966).

16. Poots, G., "Heat Transfer by Laminar Free Convection in Enclosed Plane Gas Layers", Quart. J. Mech. and Appl. Math., 11, Part 3, pp. 257-273, (1958).

17. Wilkes, J.O. and Churchill, S.W., "The Finite Difference Computation in a Rectangular Enclosure", AICHE Jour., 12, pp. 161-166, (1966).

18. Elder, J.W., "Numerical Experiments with Free Convection in a Vertical Slot", J. Fluid Mech. 24, part 4, pp. 823-843, (1966).

19. DeVahl Davis, G., "Laminar Natural Convection in an Enclosed Rectangular Cavity", Int. J. Heat Mass Transfer, 11, pp. 1675-1693, (1968).

20. MacGregor, R.K. and Emery, A.F., "Free Convection Through Vertical Plane Layers - Moderate and High Prandtl Number Fluids", J. Heat Transfer, 91, pp. 391-403, (Aug. 1969).

21. Newell, M.E. and Schmidt, F.W., "Heat Transfer by Laminar Natural Convection Within Rectangular Enclosrues", J. Heat Transfer, 92, No. 1, pp. 159-168, (1970).

22. Quon, C., "High Rayleigh Number Convection in an Enclosure - A Numerical Study", Phys. Fluids, 15, No. 1, pp. 12-19, (1972).

23. Taylor, C. and Ijan, A.Z., "A Finite Element Numerical Solution of Natural Convection in Enclosed Cavities", Computer Method in Appl. Mech. Eng. 19, pp. 429-446, (1979).

24. Boyack,B.E. and Kearney, D.W., "Heat Transfer by Laminar Natural Convection in Low Aspect Ratio Cavities", ASME Paper 72-HT-52.

25. Solan, A. and Ostrach, S., "Convection Effects in Crystal Growth by Closed-Tube Chemical Vapor Transport", Preparation and Properties of Solid State Materials, vol. 4, Marcel Dekker, Inc., N.Y., (1979).

26. Klosse, K. and Ullersma, P., "Convection in a Vapor Transport Process", J. Crystal Growth, 18, pp. 167-174, (1973).

27. Cormack, D.E., Leal, L.G. and Imberger, J., "Natural Convection in a Shallow Cavity with Differentially Heated End Walls. Part 1. Asymptotic Theory", J. Fluid Mech., 65, Part 2, pp. 209-229, (1974).

28. Cormack, D.E., Leal, L.G. and Seinfeld, J.H., "Natural Convection in a Shallow Cavity with Differentially Heated End Walls. Part 2. Numerical Solutions", J. Fluid Mech., 65, Part 2. pp. 231-246, (1974).

29. Imberger, J., "Natural Convection in a Shallow Cavity with Differentially Heated End Walls. Part 3. Experimental Results", J. Fluid Mech., 65, Part 2, pp. 247-260, (1974).

30. Bejan, A. and Tien, C.L., "Laminar Natural Convection Heat Transfer in a Horizontal Cavity with Different End Temperatures", J. Heat Transfer, 100, No. 4, pp. 641-647, (1978).

31. Ostrach, S., Loka, R.R. and Kumar, A., "Natural Convection in Low Aspect Ratio Rectangular Enclosures", in Natural Convection in Enclosures edited by Torrance and Catton and published by the Heat Transfer Division of ASME, HTD-vol.18, (1980).

32. Al-Homoud, A.A., "Experimental Study of High Rayleigh Number Convection in Horizontal Cavity with Different End Temperatures", M.S. Thesis, Univ. of Colorado, (1979).

33. Kamotani, Y., Wang, L.W. and Ostrach, S., "Experiments on Natural Convection Heat Transfer in Low Aspect Ratio Enclosures", AIAA Paper No. AIAA-81-1066, (1981), (Accepted for Publication.)

34. Sernas, V. and Lee, E.I., "Heat Transfer in Air Enclosure of Aspect Ratio Less Than One", ASME Paper 78-WA/HT-7, presented at the ASME Winter Annual Meeting, San Francisco, CA., (Dec. 1978) or J. Heat Transfer, 103, pp. 617-622, (1981).

35. Lee, E.I. and Sernas, V., "Numerical Study of Heat Transfer in Rectangular Air Enclosures of Aspect Ratio Less Than One", ASME Paper 80-WA/HT-43, presented at the ASME Winter Annual Meeting, Chicago, IL., (Nov. 1980).

36. Tseng, W., "Numerical Experiments on Free Convection in a Tilted Rectangular Enclosures of Aspect Ratio 0.5", M.S. Thesis, Report No. NIE-050, Clarkson College, Potsdam, NY, (1979);

37. Patterson, J. and Imberger, J., "Unsteady Natural Convection in a Rectangular Cavity", J. Fluid Mech., 100, part 1, pp. 65-86, (1980).

38. Simpkins, P.G. and Dudderar, T.D., "Convection in Rectangular Cavities with Differentially Heated End Walls", J. Fluid Mech., 110, pp. 433-456, (1981).

39. Shiralkar, G.S. and Tien, C.L., "A Numerical Study of Laminar Natural Convection in Shallow Cavities", J. Heat Transfer, 103, pp. 261-231, (May, 1981).

40. Jhaveri, B.S. and Rosenberger, F., "Expansive Convection in Vapor Transport across Horizontal Rectangular Enclosures", J. Crystal Growth, 56, (1982).

41. Nayfeh, A., "Perturbation Methods", chap. 6, John Wiley and Sons, (1973).

42. Ostrach, S.,"Laminar Flows with Body Forces", in High Speed Aerodynamics and Jet Propulsion [F.K. Moore, ed.], vol. 4, Chap. F, Princeton Univ. Press, Princeton, NJ, (1964).

43. Ostrach, S., "An Analysis of Laminar Free-Convection Flow and Heat Transfer About a Flat Plate Parallel to the Direction of the Generating Body Force", NACA Rep. 1111, (1953).

44. Sparrow, E.M. and Gregg, J.L., "Details of Exact Low Prandtl Number Boundary-Layer Solutions for Forced and for Free Convection", NASA Memorandum 2-27-59E, (1958).

45. Utech, H.P., Brower, W.S. and Early, J.G., "Thermal Convection and Crystal Growth in Horizontal Boat: Flow Pattern, Velocity Measurement, and Solute Distribution", Crystal Growth [Ed. H.S. Peiser], pp. 201-205, Pergamon, Oxford, (1967).

APPENDIX A

Examination of the situations for which either Eq. (3.22) or Eq. (3.23) could be satisfied.

$$\frac{\partial}{\partial \zeta}\int_0^1 \psi \frac{\partial \theta}{\partial y}\, dy = 0 \tag{3.22}$$

or

$$\int_0^1 \left(\frac{\partial \psi}{\partial \zeta}\frac{\partial \theta}{\partial y} + \psi \frac{\partial^2 \theta}{\partial \zeta \partial y}\right) dy = 0 \tag{3.23}$$

(a) $\psi = 0$

This implies no flow in the core and inappropriate to the current situation.

(b) $\theta = \theta(\zeta)$

In this case, from Eq. (3.15)

$$\frac{\partial \psi}{\partial y}\frac{\partial \theta}{\partial \zeta} = 0 \tag{A.1}$$

and thus,

$$\psi = \psi(\zeta) \tag{A.2}$$

Then, from Eqs. (3.7) and (3.8)

$$\frac{d\theta}{d\zeta} = \frac{\partial^4 \psi}{\partial y^4} = 0 \tag{A.3}$$

From (A.3), we find

$$\theta = const. \tag{A.4}$$

This implies no driving force in the core, thus it is inappropriate to the current situation.

(c) $\frac{\partial \psi}{\partial \zeta} = 0, \quad \frac{\partial^2 \theta}{\partial \zeta \partial y} = 0$

In this case, ψ and θ can be represented as

$$\psi = \psi(y) \tag{A.5}$$

and

$$\theta = f(\zeta) + g(y) \tag{A.6}$$

Substitution of (A.5) and (A.6) into Eqs. (3.7) and (3.8) yields

$$f'(\zeta) = \psi^{iv}(y) \tag{A.7}$$

Comparing both sides, the equality can be made when each side has constant value. Denoting the constant by A_1, from (A.5), (A.6) and (A.7), we find

$$\theta = A_1 \zeta + g(y) \tag{A.8}$$

$$\psi = A_1 h(y) \tag{A.9}$$

Eqs. (A.8) and (A.9) show that the temperature distribution in the core is linear and stratified, while the core flow pattern is parallel.

(d) $\psi \frac{\partial \theta}{\partial y} = G(y)$

Considering the boundary conditions (2.9b), we expect the functional form of

$$\psi = f(\zeta) g(y) \tag{A.10}$$

and $$\frac{\partial \theta}{\partial y} = f^{-1}(\zeta)\, h(y) \tag{A.11}$$

or $$\theta = f^{-1}(\zeta) P(y) + g(\zeta), \quad P(y) = \int_0^y h(y)\, dy \tag{A.12}$$

such that $$\psi \frac{\partial \theta}{\partial y} = g(y) h(y) = F(y) \tag{A.13}$$

Substituting (A.10) and (A.12) into Eq. (3.7), and from Eq. (3.8) we have

$$-\frac{f'(\zeta)}{[f(\zeta)]^2} P(y) + g'(\zeta) = f(\zeta)\, g^{iv}(y) \tag{A.14}$$

we separate the variables in (A.14) as

$$-\frac{f'(\zeta)}{[f(\zeta)]^3} = \frac{1}{P(y)}\left[g^{iv}(y) - \frac{g'(\zeta)}{f(\zeta)} \right] \tag{A.15}$$

This equation is separable if

$$\frac{g'(\zeta)}{f(\zeta)} = \text{const.} = A_2 \tag{A.16}$$

or $$P(y) = \text{const.} \tag{A.17}$$

When p(y) = const., from (A.12)

$$\theta = \theta(\zeta) \tag{A.18}$$

This situation was previously treated in case (b) and it was shown to be inappropriate to the current situation.

For the case (A.16), denoting the suitable separation constant by k, from (A.15) and (A.16)

$$g^{iv}(y) = k P(y) + A_2 \tag{A.19}$$

Let us look over (A.19) according to the values of k and A_2.

(i) k, A_2 arbitrary and non-zero

Considering the symmetry property of ψ in (2.10a),

$$\psi(\xi,\eta) = \psi(1-\xi, 1-\eta) \tag{A.20}$$

From (A.10) and (A.20),

$$f(\xi)\,g(\eta) = f(1-\xi)\,g(1-\eta) \tag{A.21}$$

We thus find

$$f(\xi) = f(1-\xi) \tag{A.22}$$

and

$$g(\eta) = g(1-\eta) \tag{A.23}$$

Also considering the symmetry property of θ in (2.10b),

$$\theta(\xi,\eta) = 1 - \theta(1-\xi, 1-\eta) \tag{A.24}$$

From (A.12) and (A.24), we then have

$$f^{-1}(\xi)P(\eta) + g(\xi) = 1 - f^{-1}(1-\xi)P(1-\eta) - g(1-\xi) \tag{A.25}$$

Since $f^{-1}(\zeta) = f^{1}(1-\zeta)$ from (A.22), we find

$$P(\eta) = -P(1-\eta) \tag{A.26}$$

and

$$g(\xi) = 1 - g(1-\xi) \tag{A.27}$$

From (A.23)

$$g^{iv}(\eta) = g^{iv}(1-\eta) \tag{A.28}$$

From (A.19) and (A.28), we thus have

$$KP(\eta) = KP(1-\eta) \tag{A.29}$$

Since from (A.26) and (A.29)

$$K P(\eta) = - K P(\eta) \tag{A.30}$$

we find

$$P(\eta) = 0 \tag{A.31}$$

Then, from (A.12)

$$\theta = g(\zeta) \tag{A.32}$$

This is identical to the case (b) which was shown to be inappropriate to the current situation

(ii) $\underline{A_2 = 0}$

In this case, from (A.16)

$$\frac{g'(\zeta)}{f(\zeta)} = 0 \tag{A.33}$$

Since θ is finite, from (A.12), $f(\zeta) \neq 0$. Thus

$$g'(\zeta) = 0 \tag{A.34}$$

and

$$g(\zeta) = const. \tag{A.35}$$

From (A.19)

$$g^{iv}(\eta) = K P(\eta) \tag{A.36}$$

Considering the symmetry properties of θ and ζ from (A.26) and (A.28) we find

$$P(\eta) = 0 \tag{A.37}$$

Then, from (A.12) and (A.33) θ = const., and this is inappropriate herein.

(iii) $\underline{k = 0}$

In this case, from (A.19), $g^{iv}(y) = A_2$, and from (A.15) and (A.16)

$$\frac{f'(\zeta)}{[f(\zeta)]^3} = 0 \tag{A.38}$$

Since $f(\zeta) \neq 0$ for finite θ in (A.12),

$$f'(\zeta) = 0 \tag{A.39}$$

and $$f(\zeta) = const. = A_3 \tag{A.40}$$

Then, from (A.16) and (A.40)

$$g'(\zeta) = A_2 f(\zeta) = A_2 A_3 = A_4 \tag{A.41}$$

and $$g(\zeta) = A_4 \zeta + A_5 \tag{A.42}$$

where A_5 is an arbitrary constant.

Substituting (A.40) and (A.42) into (A.10) and (A.12), we finally have

$$\psi = g(y) \tag{A.43}$$

and $$\theta = \frac{1}{A_3} p(y) + A_4 \zeta + A_5 \tag{A.44}$$

These are the same results obtained in the analysis of case (c).

(e) $\underline{\int_0^1 \psi \frac{\partial \theta}{\partial y} dy = 0}$

From the symmetry properties of ψ and θ,

$$\psi(y) = \psi(1-y) \tag{A.45}$$

and $$\left.\frac{\partial\theta}{\partial y}\right|_{y} = \left.\frac{\partial\theta}{\partial y}\right|_{1-y} \tag{A.46}$$

Since both $\psi(y)$ and $\frac{\partial\theta}{\partial y}$ have the same sign between y = 0 and 1, there exists no possibility of the value of the integral $\int_0^1 \psi \frac{\partial\epsilon}{\partial y}\, dy$ to be zero, unless $\psi = 0$ or $\frac{\partial\theta}{\partial y} = 0$ (i.e., $\epsilon = \epsilon(\zeta)$) in which case it was already shown to be inappropriate in the case (a) and case (b), respectively.

(f) $$\underline{\frac{\partial\psi}{\partial\zeta}\frac{\partial\theta}{\partial y} = -\psi\frac{\partial^2\theta}{\partial\zeta\partial y}} \tag{A.47}$$

Considering the boundary conditions (2.9b), ψ and θ can be expressed as

$$\psi = f(\zeta)\, g(y) \tag{A.48}$$

and $$\theta = F(\zeta)\, G(y) \tag{A.49}$$

Substituting (A.48) and (A.49) into (A.47) and dividing each side by $f(\zeta)g(y)F(\zeta)G(y)$, we then have

$$\frac{f'(\zeta)}{f(\zeta)} = -\frac{F'(\zeta)}{F(\zeta)} \tag{A.50}$$

Integration of (A.50) yields

$$\ln f = -\ln F + \ln A_6 \tag{A.51}$$

or $$f = \frac{A_6}{F} \tag{A.52}$$

where A_6 is an integration constant.

From (A.49) and (A.52), we find

$$\theta = A_6 \frac{G(y)}{f(s)} \tag{A.53}$$

From (A.24) and (A.53)

$$A_6 \frac{G(y)}{f(s)} = 1 - A_6 \frac{G(1-y)}{f(1-s)} \tag{A.54}$$

Since from (A.20) and (A.48)

$$f(s) = f(1-s) \tag{A.55}$$

from (A.54) and (A.55), we then have

$$A_6 \frac{G(y)}{f(s)} = 1 - A_6 \frac{G(1-y)}{f(s)} \tag{A.56}$$

or
$$A_6 [G(y) + G(1-y)] = f(s) \tag{A.57}$$

Comparing both sides, the equality can be made only when each side has a constant value. Denoting the constant by A_7, from (A.48) and (A.57) we find

$$\psi = A_7 g(y) \tag{A.58}$$

From (A.47) and (A.49), this gives

$$F'(s) G'(y) = 0 \tag{A.59}$$

and thus
$$F(s) = const. \tag{A.60}$$

or
$$G(y) = const. \tag{A.61}$$

The situation (A.60) represents no driving force in the core and the situation (A.61) reduces to Case (b). This case, therefore, does not show any possible core configurations.

APPENDIX B

Examination of the situations for which either Eq. (3.78) or Eq. (3.79) in Case II could be satisfied.

$$\frac{\partial}{\partial \zeta}\int_0^1 \psi \frac{\partial \theta}{\partial y}\, dy = 0 \tag{3.75}$$

or $$\int_0^1 \left(\frac{\partial \psi}{\partial \zeta}\frac{\partial \theta}{\partial y} + \psi \frac{\partial^2 \theta}{\partial \zeta \partial y} \right) dy = 0 \tag{3.76}$$

(a) $\psi = 0$

This means no flow in the core and it is inappropriate to the current situation

(b) $\theta = \theta(\zeta)$

In this situation, from Eq. (3.74)

$$\frac{\partial \theta}{\partial \zeta}\frac{\partial \psi}{\partial y} = 0 \tag{B.1}$$

and thus, $$\psi = \psi(\zeta) \tag{B.2}$$

Then from Eqs. (3.67) and (3.69), for $A^2 << 1$

$$\frac{d\theta}{d\zeta} = 0 \tag{B.3}$$

and $$\theta = const. \tag{B.4}$$

This implies no driving force in the core, thus it is inappropriate to the current situation.

(c) $\frac{\partial \psi}{\partial \zeta} = 0, \frac{\partial^2 \theta}{\partial \zeta \partial y} = 0$

In this situation, ψ and θ can be represented as

$$\psi = \psi(y) \tag{B.5}$$

and

$$\theta = f(x) + g(y) \tag{B.6}$$

Substitution of (B.5) and (B.6) into Eq. (3.69) yields

$$0 = f'(x) \tag{B.7}$$

Thus,

$$const. = f(x) \tag{B.8}$$

Then, from (B.6) and (B.8)

$$\theta = const. + g(y) \tag{B.9}$$

This implies the stratification of core temperature distribution and no driving force in the core, thus it is inappropriate to the current situation.

(d) $\psi \cdot \frac{\partial \theta}{\partial y} = F(y)$

In this situation, as in the analysis of case (d) in Appendix A, if we consider the boundary conditions (2.9b), θ and ψ can be expressed as

$$\psi = f(x)\, g(y) \tag{B.10}$$

and

$$\frac{\partial \theta}{\partial y} = f^{-1}(x)\, h(y) \tag{B.11}$$

or

$$\theta = f^{-1}(x) P(y) + g(x), \quad P(y) = \int_0^y h(y)\, dy \tag{B.12}$$

so that

$$\psi \frac{\partial \theta}{\partial y} = g(y) h(y) = F(y) \tag{B.13}$$

Substituting (B.10) and (B.12) into Eq. (3.69) and from Eq. (3.67), for $A^2 << 1$, we have

$$f(\zeta)f'(\zeta)\left[g'(y)g''(y) - g(y)g'''(y)\right] = \frac{f'(\zeta)}{f(\zeta)}P(y) + g'(\zeta) \tag{B.14}$$

After arranging,

$$\frac{1}{P(y)}\left[\left\{g'(y)g''(y) - g(y)g'''(y)\right\} - \frac{g'(\zeta)}{f(\zeta)f'(\zeta)}\right] = \frac{1}{[f(\zeta)]^3} \tag{B.15}$$

This equation is separable if

$$P(y) = const. \tag{B.16}$$

or

$$\frac{g'(\zeta)}{f(\zeta)f'(\zeta)} = const. \tag{B.17}$$

When p(y) = const., from (B.12) $\theta = \theta(\zeta)$. This situation is shown to be inappropriate to the current situation in case (b). For the case (B.17), denoting the separation constant by k in (B.15), from the second expression

$$f(\zeta) = K^{-1/3} = const. \tag{B.18}$$

Then from (B.10) and (B.12),

$$\Psi = K^{-1/3}g(y) \tag{B.19}$$

and

$$\theta = K^{1/3}P(y) + g(\zeta) \tag{B.20}$$

Substitution of (B.18) into (B.14) yields

$$g'(\zeta) = const. \tag{B.21}$$

thus, $$g(\zeta) = const. \tag{B.22}$$

This is also consistant with the result which can be obtained from (B.17) and (B.18). From (B.20) and (B.21), θ then becomes

$$\theta = K^{*} P(y) + const. \tag{B.23}$$

This shows that the core temperature distribution is stratified and it does not provide any driving force for the core flow. It is thus inappropriate to the current situation.

(e) $\int_0^1 \psi \frac{\partial \theta}{\partial y} dy = 0$

By the same reasoning of case (e) in Appendix A, this does not show any possible core configurations.

(f) $\frac{\partial \psi}{\partial \zeta} \frac{\partial \theta}{\partial y} = -\psi \frac{\partial^2 \theta}{\partial \zeta \partial y}$

By the same procedure of case (f) in Appendix A, this case reduces to the case (c) which does not show any possible core configurations appropriate to the current situation.

APPENDIX C

Consideration on the Possible Core Configurations from Eqs. (3.110)

From Eq. (3.110), outside the horizontal thermal layer two possible core temperature profiles can be obtained, i.e., θ_c = const. and $\theta_c = \theta_c(y)$. Amont them $\theta_c = \theta_c(y)$ is a possible one, thus we are going to examine whether θ_c = const. is also possible core temperature profile. For the analysis, we develop simple integral relation which can describe the core configurations.

By introducing the transformation (C.1)

$$y = \frac{1}{A\,Ra_m^{*}}\,\tilde{y} \tag{C.1}$$

into Eq. (3.100), the core energy equation within the horizontal thermal layer becomes

$$\frac{\partial(\theta,\psi)}{\partial(\xi,\tilde{y})} = A^{*}\frac{\partial^{2}\theta}{\partial\xi^{2}} + \frac{\partial^{2}\theta}{\partial\tilde{y}^{2}} \tag{C.2}$$

Rewriting Eq. (C.2), we have

$$\frac{\partial}{\partial\xi}\left(\theta\frac{\partial\psi}{\partial\tilde{y}} - A^{*}\frac{\partial\theta}{\partial\xi}\right) = \frac{\partial}{\partial\tilde{y}}\left(\theta\frac{\partial\psi}{\partial\xi} + \frac{\partial\theta}{\partial\tilde{y}}\right) \tag{C.3}$$

Integration of Eq. (C.3) with respect to $\tilde{y}$ between 0 and ∞, i.e., between the horizontal wall and mid-core region (i.e., outside the horizontal thermal layer), yields

$$\frac{\partial}{\partial\xi}\left[\int_0^{\infty}\theta\frac{\partial\psi}{\partial\tilde{y}}\,d\tilde{y} - A^{*}\int_0^{\infty}\frac{\partial\theta}{\partial\xi}\,d\tilde{y}\right] = \frac{\partial}{\partial\tilde{y}}\int_0^{\infty}\left(\theta\frac{\partial\psi}{\partial\xi}+\frac{\partial\theta}{\partial\tilde{y}}\right)d\tilde{y} \tag{C.4}$$

The left side is integrated by parts and we then have

$$\frac{\partial}{\partial \zeta}\left[\theta\psi\Big|_0^\infty - \int_0^\infty \psi \frac{\partial\theta}{\partial\tilde{y}}\, d\tilde{y}\right] = \theta\frac{\partial\psi}{\partial\zeta}\Big|_0^\infty + \frac{\partial\theta}{\partial\tilde{y}}\Big|_0^\infty + A^2\int_0^\infty \frac{\partial\theta}{\partial\zeta}\, d\tilde{y} \tag{C.5}$$

and after arranging

$$\frac{\partial}{\partial \zeta}\left[\theta_c\psi_c - \theta_w\psi_w - \int_0^\infty \psi \frac{\partial\theta}{\partial\tilde{y}}\, d\tilde{y}\right] = \theta_c\frac{\partial\psi_c}{\partial\zeta} - \theta_w\frac{\partial\psi}{\partial\zeta}\Big|_{\tilde{y}=0} + \frac{\partial\theta}{\partial\tilde{y}}\Big|_{\tilde{y}\to\infty} - \frac{\partial\theta}{\partial\tilde{y}}\Big|_{\tilde{y}=0} + A^2\frac{\partial}{\partial\zeta}\int_0^\infty \frac{\partial\theta}{\partial\zeta}\, d\tilde{y} \tag{C.6}$$

where

$$\theta_c = \theta|_{\tilde{y}\to\infty}\ ,\quad \theta_w = \theta|_{\tilde{y}=0}$$
$$\psi_c = \psi|_{\tilde{y}\to\infty}\ ,\quad \psi_w = \psi|_{\tilde{y}=0} \tag{C.7}$$

and subscripts c and w represent the horizontal wall and mid-core, respectively.

By applying the boundary conditions (2.9b) at horizontal boundaries, Eq. (C.6) reduces to

$$\frac{\partial}{\partial \zeta}\left[\theta_c\psi_c - \int_0^\infty \psi \frac{\partial\theta}{\partial\tilde{y}}\, d\tilde{y}\right] = \theta_c\frac{\partial\psi_c}{\partial\zeta} + \frac{\partial\theta}{\partial\tilde{y}}\Big|_{\tilde{y}\to\infty} + A^2\frac{\partial}{\partial\zeta}\int_0^\infty \frac{\partial\theta}{\partial\zeta}\, d\tilde{y} \tag{C.8}$$

Carrying out the derivatives on left side and after rearranging, we finally have

$$\psi_c\frac{\partial\theta_c}{\partial\zeta} - \frac{\partial}{\partial\zeta}\int_0^\infty \psi\frac{\partial\theta}{\partial\tilde{y}}\, d\tilde{y} = \frac{\partial\theta}{\partial\tilde{y}}\Big|_{\tilde{y}\to\infty} + A^2\frac{\partial}{\partial\zeta}\int_0^\infty \frac{\partial\theta}{\partial\zeta}\, d\tilde{y} \tag{C.9}$$

The integral equation (C.9) describe the core configuration.

Substitution of θ_c = const. into Eq. (C.9) then yields

$$-\frac{\partial}{\partial \zeta}\int_0^\infty \psi \frac{\partial \theta}{\partial \tilde{y}}\, d\tilde{y} = A^* \frac{\partial}{\partial \zeta}\int_0^\infty \frac{\partial \theta}{\partial \zeta}\, d\tilde{y} \qquad (C.10)$$

For $A^2 << 1$, Eq. (C.10) reduces to

$$\frac{\partial}{\partial \zeta}\int_0^\infty \psi \frac{\partial \theta}{\partial \tilde{y}}\, d\tilde{y} = 0 \qquad (C.11)$$

or $$\int_0^\infty \left(\frac{\partial \psi}{\partial \zeta}\frac{\partial \theta}{\partial \tilde{y}} + \psi \frac{\partial^2 \theta}{\partial \zeta \partial \tilde{y}} \right) d\tilde{y} = 0 \qquad (C.12)$$

Let us examine what the situations for which either Eq. (C.11) or Eq. (C.12) could be satisfied would imply.

(a) $\psi = 0$

This implies no flow within the horizontal thermal layer and thus, no flow in the core. It is thus inappropriate to the current situation because there is no heat transfer between the two ends.

(b) θ = const.

Since θ_c = const. too, the entire core remains at constant temperature. This means that no heat is transferred across the core by convection, thus it is inappropriate to the current situation.

(c) $\frac{\partial \psi}{\partial \zeta} = 0, \frac{\partial^2 \theta}{\partial \zeta \partial \tilde{y}} = 0$

In this case ψ and θ can be represented as

$$\Psi = \Psi(\tilde{y}) \tag{C.13}$$

and $$\theta = f(\xi) + g(\tilde{y}) \tag{C.14}$$

when $\hat{y} \to \infty$, from (C.14)

$$\theta|_{\tilde{y}\to\infty} = \theta_c = f(\xi) + g(\infty) \neq const. \tag{C.15}$$

Since θ_c is considered to be const. herein, this is not appropriate to the current situation.

(d) $\xi \cdot \frac{\partial \epsilon}{\partial \hat{y}} = F(\hat{y})$

Considering the boundary conditions (2.9b), we expect the functional form of

$$\Psi = f(\xi)\, g(\tilde{y}) \tag{C.16}$$

and $$\frac{\partial \theta}{\partial \tilde{y}} = f^{-1}(\xi)\, h(\tilde{y}) \tag{C.17}$$

so that $$\Psi \frac{\partial \theta}{\partial \tilde{y}} = g(\tilde{y})\, h(\tilde{y}) = F(\tilde{y}) \tag{C.18}$$

In this situation, from (C.17)

$$\theta = f^{-1}(\xi)\, P(\tilde{y}) + g(\xi) \tag{C.19}$$

with $$P(y) = \int_0^{\tilde{y}} h(\tilde{y})\, d\tilde{y} \tag{C.20}$$

when $\hat{y} \to \infty$, from (C.19)

$$\theta|_{\xi\to\infty} = \theta_c = f^{-1}(\xi)\,P(\infty) + g(\xi) \neq \text{const.} \qquad (C.21)$$

Thus, this is also inappropriate to the current situation.

(e) $\int_0^\infty \psi \frac{\partial \theta}{\partial \hat{y}}\, d\hat{y} = 0$ (C.22)

Considering the symmetry properties of ψ and θ, as can be inferred from the case (e) of Appendix A, ψ and $\frac{\partial \theta}{\partial \hat{y}}$ are either increasing or decreasing between the horizontal wall and the mid-core region. Thus, there is no reason that the integral in (C.22) becomes zero, unless $\psi = 0$ or $\frac{\partial \theta}{\partial \hat{y}} = 0$, i.e., $\theta = \theta(\xi)$ or const., in which case it was shown to be inappropriate to the current situation in case (a) and case (b), respectively.

From the considerations made above, it is shown that θ_c = const. is not a possible core temperature profile herein. However, from Eq. (C.10), when A^2 is not negligibly small, i.e., for $A^2 \sim O(1)$, the right expression in Eq. (C.10) is not negligible and Eq. (C.10) itself can be satisfied for a suitable distribution of θ within the horizontal thermal layer. Thus, θ_c = const. in this situation can also be a possible core temperature profile. This means that heat is transferred by convection across the cavity through the horizontal thermal layer while the mid-core region remains at constant temperature.

APPENDIX D

Modified Characteristic Stream Function $\bar{\Psi}_R$

In the boundary layer equations, in normalizing the velocity components within the thermal or flow boundary layers we use the same characteristic velocity, U_R, because the characteristic velocity is of the same order of magnitude within both boundary layers. On the contrary, in vorticity transport equations of the boundary layer, since the characteristic stream function is represented as

$$\Psi_R \sim \tilde{\ell}\, U_R \tag{D.1}$$

where $\tilde{\ell}$ is the characteristic length , even for the same value of U_R, the characteristic stream function changes according to the characteristic length scale, $\tilde{\ell}$, and thus one should be careful in normalizing the vorticity equations. Actually, in the case of large Prandtl numbers, the flow boundary layer extends beyond the thermal boundary layer, thus the characteristic stream function differs within each layer and it needs to be determined according to the corresponding boundary layers. For low Prandtl numbers, however, although the thermal boundary layer extends beyond the flow boundary layer, since the main body of fluid flows within the flow boundary layer, the characteristic stream function will be of the same order within both boundary layers. In Eq. (3.89), the

estimate of the characteristic stream function, Ψ_R, was made for the thermal boundary layer, say δ_t, for Pr $\gtrsim$ 1 (including Pr >> 1). Based on the above arguement, for the same Prandtl numbers, we now determine the characteristic stream function, $\bar{\Psi}_R$, for the flow boundary layer.

From (D.1), U_R can be written as

$$U_R \sim \frac{\Psi_R}{\delta_t} = \frac{\Psi_R}{\delta_f}\frac{\delta_f}{\delta_t} = \frac{\bar{\Psi}_R}{\delta_f} \tag{D.2}$$

where $\bar{\Psi}_R = \frac{\delta_f}{\delta_t}\ \Psi_R$, is the characteristic stream function modified for the flow boundary layer, δ_f. To estimate $\bar{\Psi}_R$, we replace Ψ_R by $\bar{\Psi}_R$ in Eq. (2.13) and introduce the multiple scales for the flow boundary layer, δ_f, as

$$\zeta = x,\ \eta = \frac{x}{\bar{\varepsilon}_x} \tag{D.3}$$

where $$\bar{\varepsilon}_x \sim \frac{\delta_f}{L} \tag{D.4}$$

Then substituting the derivatives of (D.3) into Eq. (2.13) and balancing the inertia and viscous forces within δ_f in the end, we have

$$\frac{1}{\bar{\varepsilon}_x} \sim \frac{\nu L}{\bar{\Psi}_R H}\frac{A^2}{\bar{\varepsilon}_x^2} \tag{D.5}$$

and from (D.2) and (D.5), we find

$$\bar{\varepsilon}_x \sim \frac{\nu A}{\bar{\Psi}_R} \sim \frac{\nu A}{\Psi_R}\frac{\delta_t}{\delta_f} \tag{D.6}$$

For δ_t, since from (3.85)

$$\varepsilon_x \sim \frac{\alpha A}{\Psi_R} \tag{D.7}$$

from (D.6) and (D.7), we have

$$\bar{\varepsilon}_x \sim Pr \frac{\delta_t}{\delta_f} \varepsilon_x \tag{D.8}$$

or $$\frac{\bar{\varepsilon}_x}{\varepsilon_x} \sim Pr \frac{\delta_t}{\delta_f} \tag{D.9}$$

Then, from (3.52), (D.4) and (D.9)

$$\frac{\bar{\varepsilon}_x}{\varepsilon_x} \sim \frac{\delta_t}{\delta_f} \sim Pr \frac{\delta_t}{\delta_f} \tag{D.10}$$

and thus, $$\frac{\delta_f}{\delta_t} \sim Pr^{\frac{1}{2}} \tag{D.11}$$

Since from (3.91)

$$\delta_t \sim \frac{H}{Ra_H^{\frac{1}{4}}} \tag{D.12}$$

from (D.11) and (D.12), we find

$$\delta_f \sim \frac{Pr^{\frac{1}{2}}}{Ra_H^{\frac{1}{4}}} H \tag{D.13}$$

and thus, $$\bar{\Psi}_R = \frac{\delta_f}{\delta_t} \Psi_R \sim \alpha Pr^{\frac{1}{2}} Ra_H^{\frac{1}{4}} \tag{D.14}$$

With this modified characteristic stream function, $\bar{\Psi}_R$, in (D.14), the estimate of the horizontal viscous layer was made in (3.119).


DAT
ILM